

# Evaluation of CLZ1 as a Biomarker for Neurological Tumours

Natasha Falkingham



Division of Biological and Life Sciences  
Faculty of Health and Medicine  
Lancaster University

Thesis Submitted for Degree of Master of Science by Research,  
August 2020

## **Declaration**

This dissertation is the result of my own work and includes nothing, which is the outcome of work done in collaboration except where specifically indicated in the text. It has not been previously submitted, in part or whole, to any university or institution for any degree, diploma, or other qualification.

Natasha Falkingham

## **Abstract**

Glioblastoma is most common type of brain tumour with an extremely poor prognosis due to lack of effective treatment options. CIZ1, a protein found to be implicated in a range of cancers, has been identified as a potential biomarker. CIZ1 has a role in the replication of DNA and cell cycle control through the coordination of cyclin A and E within the nucleus. This study will evaluate the use of CIZ1 as a biomarker in advanced glioblastoma. Immunohistochemistry showed that CIZ1 expression is increased in 6/6 FFPE tissue sections. In FFPE patient samples CIZ1 is expressed primarily in the cytoplasm, and that its expression can be used to distinguish between normal and tumour cells. In addition, using primary glioblastoma cells (BTNW914) depletion of CIZ1 reduced proliferation, suggesting that CIZ1 may promote tumour growth. Furthermore, preliminary evidence demonstrates that CIZ1 levels can be reduced by inhibition of CDK and DDK inhibitors that reduce CIZ1 levels in vitro. These results suggest that CIZ1 could be a potential useful diagnostic and prognostic biomarker and a target for therapeutic intervention.

## **Acknowledgements**

Firstly, I would like to thank my supervisor Dr Nikki Copeland for his unending support, patience and guidance throughout this whole experience.

I would like to thank Dr Timothy Dawson and Katherine Ashton at Royal Preston Hospital for their knowledge and assistance with the BTNW patient samples. Thank you also to my co-supervisor Dr Sarah Allinson for advice when needed.

I would also like to thank the friends I have made on this journey, with special thanks to Freya Ferguson and James Tollitt. Thank you, Freya, for your wonderful kindness, support and positivity. Thank you, James, for your humour, teaching of lab techniques and answering the many, many questions I had.

I would like to give a massive thank you to my partner, Jordan Cartmell, for the incredible support and motivation to continue when I needed it most. Thank you also to my parents, Leonia and David Falkingham. Without their continuous emotional support, I would never have achieved this much.

## Abbreviations

Abbreviation	Full Term
ATRX	ATP dependent helicase or X-linked helicase II
BRAF	B-Raf proto-oncogene, serine/threonine kinase
CDK	Cyclin Dependent Kinase
CDKi	Cyclin dependent kinase inhibitors
CDKN2A	cyclin dependent kinase inhibitor 2A
CIZ1	Cip1-Interacting Zinc Finger Protein
CT	Computed tomography
CTL	Cytotoxic T-lymphocyte
CTLA-4	Cytotoxic T-lymphocyte-associated protein 4
CVT	CVT-313
DAPI	4',6-Diamidino-2-Phenylindole
DDK	Dbf4 Dependent Kinase (Cdc7 - Dbf4)
DDKi	DBF4-dependent kinase inhibitor
DMEM	Dulbecco's Modified Eagle Medium
DNA	Deoxyribonucleic Acid
EdU	Ethynyl Deoxyuridine
EGFR	Epidermal Growth Factor Receptor
EGFRBi	EGFR bispecific antibody
EMEM	Eagle's Minimum Essential Medium
HCC	Hepatocellular carcinoma
hTERT	Human Telomerase reverse transcriptase
IDH	Isocitrate Dehydrogenase
MDM2	Mouse Double Minute 2 Homolog
MET	MET proto-oncogene, receptor tyrosine kinase
MGMT	O6-methylguanine-DNA methyltransferase
MH3	Matrin 3 type zinc finger
MRI	Magnetic resonance imaging
NF1	Neurofibromin 1
NICE	The National Institute For Health And Care Excellence
ORC	Origin replication complex
PARP	Poly(ADP-ribose)polymerase
PD	Palbociclib (PD0332991) Isethionate
PDGF-A	Platelet-derived growth factor subunit A
PDGFRA	Platelet Derived Growth Factor Receptor Alpha
PET	Positron emission tomography
PHA	PHA-767491 dihydrochloride
PTEN	Phosphatase And Tensin Homolog
RNA	Ribonucleic Acid
Ros	Roscovitine
SDS	Sodium Dodecyl Sulfate
SDS-PAGE	SDS-Polyacrylamide Gel Electrophoresis
TAZ	YAP/Tafazzin

<b>TMZ</b>	Temozolomide
<b>TP53</b>	Tumour protein p53
<b>TTFs</b>	Tumour treating fields
<b>UPS</b>	Ubiquitin/Proteasome System
<b>WHO</b>	World Health Organisation
<b>XL</b>	XL-413 hydrochloride
<b>YAP</b>	Yes associated protein

## Contents

Abstract.....	1
Acknowledgements .....	2
Abbreviations.....	3
Chapter 1: Introduction.....	8
1.1 Introduction.....	9
1.2 Glioblastoma .....	9
1.2.1 Epidemiology .....	9
1.2.2 Genetic and Molecular pathogenesis .....	10
1.2.3 Diagnosis and Early Detection .....	12
1.2.4 Current and potential future treatments .....	13
1.3 CIZ1 .....	16
1.3.1 CIZ1 Discovery .....	16
1.3.2 CIZ1 function in initiation of DNA replication and cell cycle regulation .....	16
1.3.3 Role of CIZ1 in tumourigenesis .....	20
1.4 Aims .....	22
Chapter 2: Methods and Materials .....	23
2.1 Cell Culture.....	24
2.2 Primary Cells .....	24
2.3 Antibodies.....	24
2.4 Sodium Dodecyl Sulphate Polyacrylamide Gel Electrophoresis (SDS-PAGE) .....	26
2.5 Western Blotting .....	26
2.6 Standardising Protein Loads.....	27
2.7 Drug treatments.....	27
2.8 Flow Cytometry.....	28
2.9 Determination of Percentage S-phase Cells by Ethynyl Deoxyuridine (EdU) Incorporation .....	29
2.10 Nucleofection of cell lines .....	29
2.11 RNA extraction and qPCR .....	29
2.12 Sub-Cellular Fractionation .....	30
2.13 Immunohistochemistry of BTNW patient samples.....	30
2.13.1 Antigen Retrieval.....	30
2.13.2 Immunostaining using the Vectastain Elite Universal ABC Kit .....	31
2.14 Ethics Statement for use of Patient Samples and Primary Cells .....	32
Chapter 3: Determination of CIZ1 localisation and expression in glioblastoma.....	33
3.1 Introduction.....	34
3.2 Immunohistochemistry using polyclonal CIZ1 antibodies .....	35
3.2.1 Antibody Optimisation .....	35

3.2.2 Observed CIZ1 staining in normal tissues is limited to specific cell types .....	37
3.2.3 Basic cancer morphology .....	38
3.2.4 CIZ1 overexpression and specificity in patient IHC samples .....	41
3.2.5 Micrometastases and Invasion .....	43
3.3 Localisation and expression of CIZ1 in neural cell lines .....	44
3.3.1 Fractionation of neural cell lines .....	44
3.3.2 Immunofluorescence of neural cells .....	46
3.4 Chapter Discussion .....	50
3.4.1 CIZ1 appears to be a biomarker for glioblastoma and identifies tumour margins and micrometastasis .....	50
3.4.2 Localisation of CIZ1 .....	52
Chapter 4: Modulation of CIZ1 expression with CDK and DDK small molecule inhibitors....	55
4.1 Introduction.....	56
4.2 Transfecting Neural Cells .....	58
4.2.1 BTNW914 transfection optimisation .....	58
4.2.2 CIZ1 depletion effects .....	61
4.3 Reduction of CIZ1 levels by CDK/DDK inhibition .....	64
4.3.1 Proof of principle using SW620 cells .....	64
4.3.2 Neural cells .....	68
4.4 Chapter Discussion .....	73
4.4.1 Knockdown of CIZ1 reduces proliferation and cell cycle progression .....	73
4.4.2 CDK and DDK inhibitors reduce CIZ1 and proliferation .....	74
Chapter 5: General Discussion .....	77
5.1 Implications of the work .....	78
5.2 Limitations and future work.....	78
5.3 Concluding remarks.....	80
References .....	82

## Figures and Tables Contents

### Figures

Figure 1.1: Initiation of DNA replication. ....	18
Figure 1.2: Cyclin-CDK control of the cell cycle. ....	19
Figure 3.1: Optimisation of CIZ1 antibody for immunohistochemistry. ....	36
Figure 3.2: CIZ1 staining of neurons in healthy tissue. ....	37
Figure 3.3: Differential staining of endothelial cells. ....	38
Figure 3.4: CIZ1 staining of gemistocytic astrocytes. ....	39
Figure 3.5: Oedema within tumour section. ....	40
Figure 3.6: Multipolar cells are characteristic of glioblastoma. ....	41
Figure 3.7: Representative anti-CIZ1 IHC of FFPE sections. ....	42
Figure 3.8: Brain surface with pia vessel infiltrating from pia mater at two magnifications. ....	43
Figure 3.9: Areas of tumour heterogeneity within a glioblastoma tumour area. ....	44
Figure 3. 10: Fractionation of neural cell lines. ....	46
Figure 3.11: Optimisation of CIZ1 antibody for immunofluorescence with BTNW914 cells. ....	47
Figure 3.12: Optimisation of CIZ1 antibody for immunofluorescence with SVGp12 cells. ....	48
Figure 3.13: Representative immunofluorescence images of BTNW914 and SVGp12 cells. ....	49
Figure 4.1: Model of CIZ1 regulation CDK2 and DDK kinase activity and UPS mediated degradation. ....	57
Figure 4.2: Immunofluorescent images of GFP transfected BTNW914 cells. ....	60
Figure 4.3: Anti-CIZ1 siRNA transfection of BTNW914 cells. ....	62
Figure 4.4: Treating SW620 cells with CDKis and DDKis. ....	67
Figure 4.5: Treating BTNW914 cells with CDKis and DDKis. ....	69
Figure 4.6: Treating U87MG cells with CDKis and DDKis. ....	71
Figure 4.7: Treating SVGp12 cells with CDKis and DDKis. ....	72

### Tables

Table 1.1: WHO classification of glioblastoma tumours. ....	11
Table 1.2: The Cancer Genome Atlas classification of glioblastoma tumours. ....	12
Table 2.1: Antibodies used in this study. ....	25
Table 2.2: Small molecule kinase inhibitors used in this study. ....	28
Table 4.1: Percentage of GFP transfected BTNW914 cells per program. ....	61
Table 4.2: Summary of small molecule inhibitors used. ....	65

# **Chapter 1: Introduction**

## **1.1 Introduction**

Gliomas are the most common type of brain cancer, which are believed to arise from the neuroepithelial group of cells, which include neural stem cells (NSCs), astrocytes or oligodendrocyte precursor cells, although there is some debate regarding this in literature. The World Health Organisation (WHO) classifies astrocytic gliomas based on histologic criteria from low-grade lesions (grades I–II) to high-grade (grades III–IV) malignancies. Glioblastoma is classified as grade IV. Glioblastoma is the most common and most aggressive malignant brain tumour with a 5.1% 5-year survival rate (Ostrom et al., 2015) and a ~10 month median survival (Zhu et al., 2017). There are currently no effective treatments, therefore there is an unmet clinical need to identify new therapeutic targets and develop more effective treatments.

Cip1-interacting zinc-finger protein 1 (CIZ1) is a protein found to be implicated in a range of cancers, with a role in promoting tumour growth. Here we aim to identify whether CIZ1 is expressed in glioblastoma, to determine if its expression is altered in glioblastoma, and to establish if reduction in CIZ1 levels reduces primary glioblastoma cell line proliferation. The literature review here will provide an overview of glioblastoma, its clinical manifestation and molecular biomarkers. In addition, an overview of CIZ1 function in normal cell proliferation and cancer biology will be described.

## **1.2 Glioblastoma**

### **1.2.1 Epidemiology**

Glioblastoma is the most common type of brain tumour, with an incidence rate of 3.19 in 100,000 (Thakkar et al., 2014) and a global incidence rate of approximately 10 in 100,000 (Iacob and Dinca, 2009). Additionally, there is evidence that incidence is increasing further, with studies showing a similar percentage rise across different age groups, despite the large

differences in number of cases for each group, which suggests a widespread environmental factor may be responsible (Dobes et al., 2011, Philips et al., 2018).

Glioblastoma accounts for 50% of all gliomas in all age groups (Rock et al., 2012). It can occur at any age, but the peak incidence occurs between 75 to 79 years (Thakkar et al., 2014, Li et al., 2018). The ratio of glioblastoma incidence is higher in men compared to women, with a 3:2 M:F ratio (Ohgaki and Kleihues, 2005, Thakkar et al., 2014). Caucasians are affected more frequently than other ethnicities: Europe and North America 3-4 per 100,000 whereas Asia 0.59 per 100,000 (Louis et al., 2016). Glioblastoma patients have a poor prognosis with a 1-year post-diagnosis survival rate of 37.2%, a 2 year survival rate of 13.7%, and a 5-year survival rate of 5.1% (Ostrom et al., 2015, Thakkar et al., 2014). Median survival post-diagnosis is approximately 10 months (Zhu et al., 2017).

### **1.2.2 Genetic and Molecular pathogenesis**

Traditionally, glioblastomas have been divided into primary and secondary tumours. In the current (2016) World Health Organisation (WHO) classification of CNS tumours, glioblastomas are characterised into two main groups: Isocitrate dehydrogenase (IDH) wild-type which correlates closely with primary glioblastoma, and IDH mutant, which correlates closely with secondary glioblastoma (Louis et al., 2016). A third classification exists whereby IDH status is unavailable or indeterminate, therefore is classified as glioblastomas NOS (not otherwise specified) (Table 1.1).

Primary glioblastomas are those that arise de novo, accounting for 90% of all glioblastomas. Primary glioblastomas are the more aggressive type and they tend to occur in elderly patients, with a mean age of 62 years. They often have amplification of Epidermal Growth Factor Receptor (EGFR), overexpression of Mouse Double Minute 2 Homolog (MDM2) and mutation in Phosphatase And Tensin Homolog (PTEN) (Ohgaki and Kleihues, 2013). Three

glioblastoma histological variants are recognised: giant cell glioblastoma, gliosarcoma and epithelioid glioblastoma (Louis et al., 2016).

Secondary glioblastomas, in contrast, are those which arise from a pre-existing lower grade diffuse astrocytoma or anaplastic astrocytoma, generally identifiable by their IDH mutant status. They are relatively uncommon, only accounting for approximately 10% of all glioblastomas. These tumours tend to be less aggressive than primary glioblastomas and they tend to occur in younger patients (Louis et al., 2016, Ohgaki and Kleihues, 2013). Secondary glioblastomas also demonstrate p53 mutations, amplification of Platelet-Derived Growth Factor Subunit A (PDGF-A), loss of heterozygosity of chromosomes 10q and 17p, loss of 19q and increased telomerase activity and Human Telomerase Reverse Transcriptase (hTERT) expression (Ohgaki and Kleihues, 2013). They are almost always O6-methylguanine-DNA methyltransferase (MGMT) methylated (Mulholland et al., 2012).

<b>WHO classification</b>	<b>Markers</b>
Primary glioblastoma	Wildtype IDH EGFR amplification MDM2 overexpression PTEN mutation
Secondary glioblastoma	IDH mutation p53 mutation PDGF-A amplification Loss of heterozygosity of chromosomes 10q and 17p 19q deletion Increased telomerase activity Increased hTERT expression MGMT methylation.
NOS	No distinct markers

**Table 1.1: WHO classification of glioblastoma tumours.** Subdivision of glioblastomas based on the molecular changes (Louis et al., 2016).

Based on gene expression profiling of patient tumours, The Cancer Genome Atlas (TCGA) analysis classifies glioblastoma into four subgroups: classical, mesenchymal, proneural and

neural. Each of these subtypes has its own distinct signature (Verhaak et al., 2010, Cancer Genome Atlas Research, 2008) (Table 1.2). The classical subtype is categorised by the loss of cyclin dependent kinase inhibitor 2A (CDKN2A) and EGFR amplification, in addition to chromosome 7 amplification and chromosome 10 deletion. The hallmarks of proneural transcriptional subclass are Platelet Derived Growth Factor Receptor Alpha (PDGFRA), TP53 and the most frequent IDH1 mutations. Mutations neurofibromin 1 (NF1) and PTEN are the main features of mesenchymal subtype. The neural subtype currently has no unique genetic signature (Cloughesy et al., 2014, Verhaak et al., 2010).

<b>TCGA classification</b>	<b>Markers</b>
Classical	CDKN2A deletion EGFR amplification/mutation Chromosome 7 amplification Chromosome 10 deletion
Mesenchymal	NF1 mutation PTEN mutation
Proneural	IDH1 mutation PDGFRA mutation TP53 mutation
Neural	No distinct markers

**Table 1.2: The Cancer Genome Atlas classification of glioblastoma tumours.** Subdivision of glioblastomas based on the molecular changes (Verhaak et al., 2010).

### 1.2.3 Diagnosis and Early Detection

The current methods used for diagnosis are conducting brain scans, such as magnetic resonance imaging (MRI) or a computed tomography (CT) scan (Shukla et al., 2017, Miletich, 2016). Subsequently, a biopsy will then be taken to allow a more accurate diagnosis of the tumour type. Clinical presentation of symptoms such focal neurological deficit and cognitive impairment as a direct effect necrotic destruction of brain tissue, headaches due to increased intracranial pressure caused by tumour growth and increased oedema, and seizures depending on size and location of the tumour (Alexander and Cloughesy, 2017, Duhrsen et al., 2019). One of the main issues with current diagnosis techniques is that the tumour is identified already at a late stage, which contributes to poor prognosis.

Typical histological features of glioblastoma include regions of necrosis, microvascular proliferation, abundant mitoses, and pleiomorphic cells (Urbanska et al., 2014, Wen and Kesari, 2008). These features are used to assist in grading and diagnosis. According to The National Institute For Health And Care Excellence (NICE) guidelines following the latest version of the WHO classification for gliomas, the recommended molecular markers for diagnostic use include: IDH1 and IDH2 mutations, ATRX chromatin remodeler (ATRX) mutations to identify IDH mutant astrocytomas and glioblastomas, 1p/19q codeletion to identify oligodendrogliomas, histone H3.3 K27M mutations in midline gliomas and B-Raf proto-oncogene, serine/threonine kinase (BRAF) fusion and gene mutation to identify pilocytic astrocytoma (Louis et al., 2016). Other molecular markers suggested for determining prognosis and guide treatment include MGMT promoter methylation (Hegi et al., 2005, Mulholland et al., 2012) and TERT promoter mutations (Lee et al., 2017) in IDH-wildtype gliomas (Louis et al., 2016). EGFR amplification/mutation is a common feature of classical subtype (An et al., 2018, Gan et al., 2009, Struve et al., 2020). There is also work looking into the use of microRNAs as potential circulating biomarkers, which would prove extremely useful in terms of diagnosis, as being able to test without the need for a biopsy would reduce costs and time, whilst increasing safety for the patient (Tumilson et al., 2014, Hayes et al., 2015, Saadatpour et al., 2016).

#### **1.2.4 Current and potential future treatments**

There is currently no effective cure for glioblastoma, with the last breakthrough being the introduction of temozolomide initially as a second line therapy, then as a result of larger trials was approved as a front-line drug in 2007 (NICE, 2001). The current standard of treatment is surgical resection to the extent feasible, followed by adjuvant radiotherapy or chemotherapy (Stupp et al., 2005). It has been shown that temozolomide in addition to radiation for a subgroup of patients with a methylated MGMT promoter results in a modest but significant

improvement in survival (Hegi et al., 2005, Stupp et al., 2005). Despite the significant improvements seen using the Stupp protocol, resulting in 26.5% 2 year survival from a 10.4% survival seen with radiotherapy alone, glioblastoma tumours are resistant to these conventional therapies, rendering them still mostly ineffective, with a median survival rate of 15-16 months (Bi and Beroukhim, 2014).

Tumour Treating Fields (TTFs) is a research area that is gaining traction since their discovery in 2004 (Hottinger et al., 2016, Kirson et al., 2004), gaining approval for use in treatment of recurrent glioblastoma in 2011, then approved to treat newly diagnosed glioblastoma in 2015. This novel therapy applies low intensity, intermediate frequency, alternating electrical fields to damage rapidly dividing tumour cells by disrupting of cytokinesis, and interfere and prolong cell division, resulting in apoptosis (Rick et al., 2018, Burri et al., 2018). The EF-14 clinical trial was conducted to evaluate the efficacy and safety of TTFs used in combination with temozolomide maintenance treatment after chemoradiation therapy for patients with glioblastoma (Stupp et al., 2015). To investigate whether TTFs improves progression-free and overall survival of patients with glioblastoma, the EF-14 clinical trial demonstrated that adding TTFs to standard therapy improved OS (5-year OS: 13% vs 5%,  $P = .004$ ) with no negative impact on quality of life. (Stupp et al., 2017, Stupp et al., 2015). Despite approval of use, incorporation of TTFs into glioblastoma treatment has been somewhat slow, due to concerns about its cost, practicality of its usage from a patient perspective, and some slowness of the medical and scientific community to embrace its unconventional mechanism (Rick et al., 2018).

There are currently numerous ongoing clinical trials for adult glioblastoma, many of which are testing adjuvants to current treatment. Others are involved with treating symptoms, differentiating patients in response to treatment and improving diagnostic techniques. There are two ongoing studies called PARADIGM and PARADIGM-2 which are running in parallel

using Poly(ADP-ribose)polymerase (PARP) inhibitor olaparib alongside radiotherapy or radiotherapy and chemotherapy respectively (Fulton et al., 2018). PARP is an essential enzyme in base excision repair and single strand break DNA repair, which includes DNA lesions which arise from radiation treatment (del Rivero and Kohn, 2017). The safety and tolerability of olaparib with radiotherapy was confirmed by phase 1 of the PARADIGM clinical trial (Chalmers et al., 2017) in addition to three parallel phase I studies looking at different cancers (de Haan et al., 2019). Another ongoing trial currently recruiting is the Ipi-Glio trial, a phase II randomised study of ipilimumab with temozolomide versus temozolomide alone after surgery and chemoradiotherapy in patients with recently diagnosed glioblastoma (Brown et al., 2020). Ipilimumab is a monoclonal antibody which targets cytotoxic T-lymphocyte-associated protein 4 (CTLA-4), a protein receptor that downregulates the immune system (Alaia et al., 2018). Cytotoxic T lymphocytes (CTLs) can recognise and destroy cancer cells. Ipilimumab is already clinically approved for treating melanoma (Specenier, 2016), with clinical trials for prostate (Beer et al., 2017, Beer et al., 2012), small cell lung cancer (Antonia et al., 2016), non-small cell lung cancer (Hellmann et al., 2017) and bladder cancer (Galsky et al., 2018).

There are other potential avenues for glioblastoma treatment. EGFR amplification is common in the classical subtypes of glioblastoma. Several randomised phase III studies have revealed that treatment with EGFR tyrosine kinase inhibitors results in an improved progression-free survival compared to standard chemotherapy in chemo-naïve patients with advanced non-small cell lung cancer, selected based on the presence of EGFR mutations (Takeda and Nakagawa, 2019). There was a phase I/II clinical trial that had been approved which was proposing to use EGFR bispecific antibody (EGFRBi)-armed autologous T cells in treating patients with recurrent or refractory glioblastoma, which was withdrawn due to lack of funding and a primary co-investigator of the trial leaving the institution (Zitron et al., 2013).

## 1.3 CIZ1

### 1.3.1 CIZ1 Discovery

Cip1-interacting zinc-finger protein 1 (CIZ1) is a protein discovered as a novel binding partner of p21<sup>Cip1/Waf1</sup> in a yeast two-hybrid screen which used Cyclin E/p21<sup>Cip1/Waf1</sup> as bait (Mitsui et al., 1999). A region of about 150 amino acids containing the first zinc-finger motif in CIZ1 was shown to be the binding site for p21<sup>Cip1/Waf1</sup>.

CIZ1 is comprised of 842 amino acid residues, containing two glutamine-rich domains, three C2H2-type zinc finger motifs, an acidic domain, and a matrix 3 type zinc finger (MH3) domain (Mitsui et al., 1999). The C-terminal domain containing the three zinc-finger motifs and MH3 anchors CIZ1 to the nuclear matrix (Ainscough et al., 2007), where the N terminal, which contains polyglutamine repeats and glutamine-rich region, promotes DNA replication initiation but cannot bind the nuclear matrix (Coverley et al., 2005, Copeland et al., 2010). CIZ1 is associated with the nuclear matrix (Ainscough et al., 2007) and is non-essential in mice, with CIZ1 null mice showing no severe developmental defects (Nishibe et al., 2013).

### 1.3.2 CIZ1 function in initiation of DNA replication and cell cycle regulation

DNA replication is a spatially and temporally controlled to ensure that DNA replication happens once per cell cycle. This requires the formation of specific complexes: the pre-replication complex (pre-RC), pre-initiation complex (pre-IC)/helicase activation and replisome formation that enable reproducible and high-fidelity duplication of the genome. The process of pre-RC assembly begins with the origin recognition complex (ORC) binding to DNA at AT rich motifs, serving as a platform for replication machinery to bind. MCM2-7 complex loading is mediated by sequential rounds of binding and release of Cdc6 and Cdt1 (Edwards et al., 2002, Yardimci and Walter, 2014). Each round loads a single MCM2-7 complex, resulting in two MCM2-7 complexes loaded in opposing orientations that 'licenses' origins for DNA replication.

Formation of the Pre-IC is driven by cyclin E/CDK2 and DDK activity, which promotes recruitment of CDC45-MCM2-7-GINS (CMG) complex. MCM10 aids in activation of CMG via recruitment of Cdc45 and stimulating DDK phosphorylation of MCM2, which thereby leads to GINS attachment to MCM2-7 (Perez-Arnaiz et al., 2016). Also, MCM10 can aid activation through direct binding with MCM2-7 complex (Douglas and Diffley, 2016) This allows helicase activity to commence and DNA replication to begin (Figure 1.1).

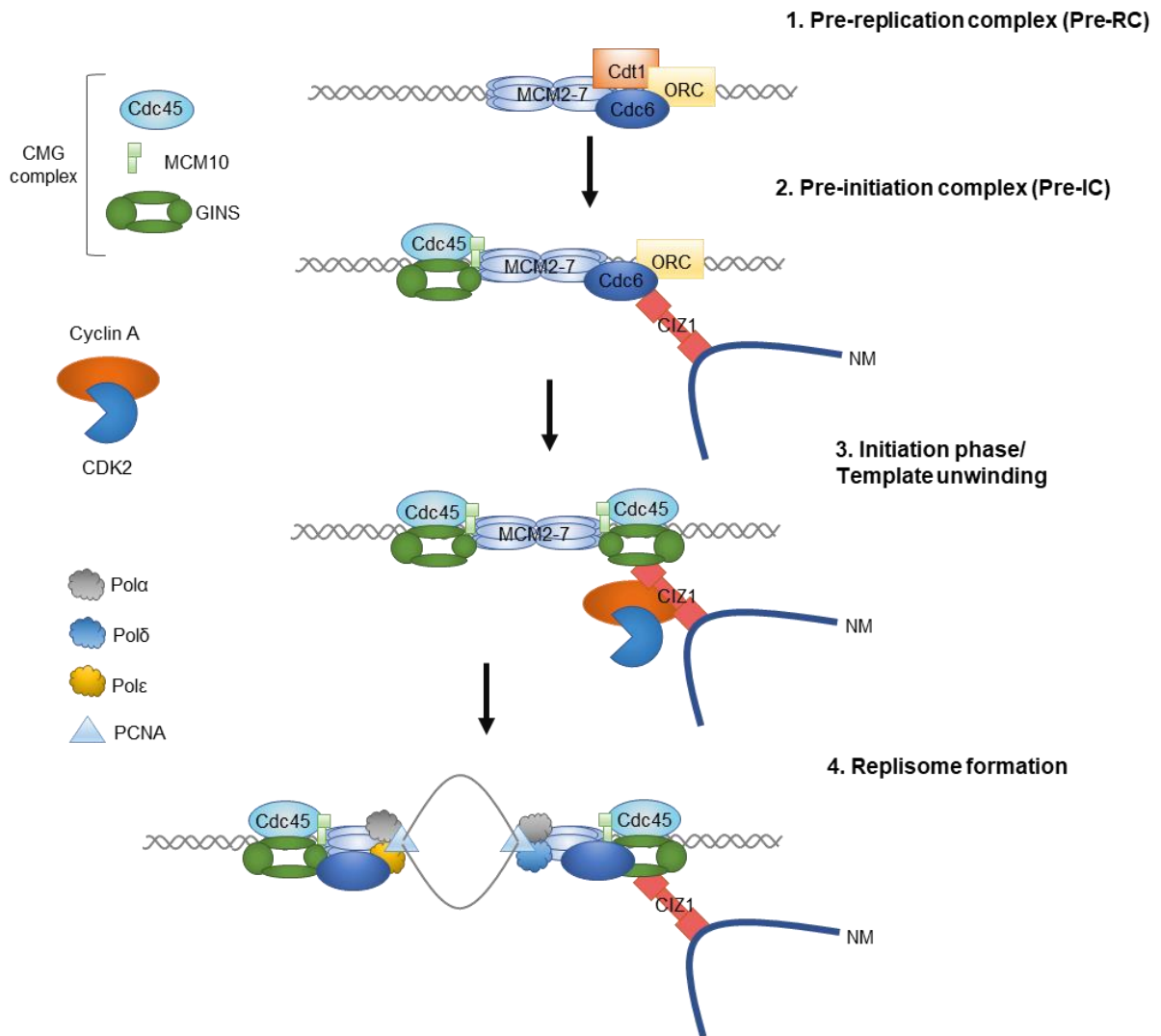


**Figure 1.1: Initiation of DNA replication.** The origin recognition complex (ORC) binds to DNA. MCM2-7 complex loading is mediated by sequential rounds of binding and release of Cdc6 and Cdt1 (Edwards et al., 2002, Yardimci and Walter, 2014). Each round loads a single Mcm2-7 complex, resulting in two Mcm2-7 complexes loaded in opposing orientations that 'licenses' origins for DNA replication. Formation of the Pre-IC is driven by cyclin E/CDK2 and DDK activity, which promotes recruitment of CDC45-MCM2-7-GINS (CMG) complex. MCM10 aids in activation of CMG via recruitment of Cdc45 and stimulating DDK phosphorylation of MCM2, which thereby leads to GINS attachment to MCM2-7 (Perez-Arnaiz et al., 2016). MCM10 aids activation through direct binding with MCM2-7 complex (Douglas and Diffley, 2016) allowing helicase activity to commence and DNA replication to begin. CIZ1 is a nuclear matrix protein binding to Cdc6 and facilitating cyclin E – CDK2 then cyclin A – CDK2 recruitment to replication complex (Copeland et al., 2015, Copeland et al., 2010, Coverley et al., 2005). Figured adapted from (Pauzaite, 2019)

The process of DNA replication is tightly regulated by CDK activity. Oscillating CDK activity seen throughout the cell cycle is important for restricting DNA replication occurs only once per cell cycle, ensuring genomic integrity is maintained, and contributes to separation of replication

licensing from replication origin firing (Figure 1.2). Pre-RC assembly begins in later mitosis in cycling cells, as CDK activity drops due to APC/C activation, cyclin degradation and phosphatase activation (Zhang et al., 2016, Fragkos et al., 2015). These events are restricted to early G1 phase while CDK activity remains low. Pre-RC assembly is inhibited during mid to late G1 phase when CDK activity rises leading to phosphorylation of pre-RC components Orc2/6, Cdc6 and Cdt1, resulting in cytosolic localisation or proteasomal degradation (Chen and Bell, 2011, Walter et al., 2016, Johansson et al., 2014, Drury et al., 2000, Mimura et al., 2004, Diril et al., 2012). If CDK activity is too high, CDK mediated phosphorylation of DNA pol  $\alpha$  prevents initiation of DNA replication (Voitenleitner et al., 1997, Voitenleitner et al., 1999).

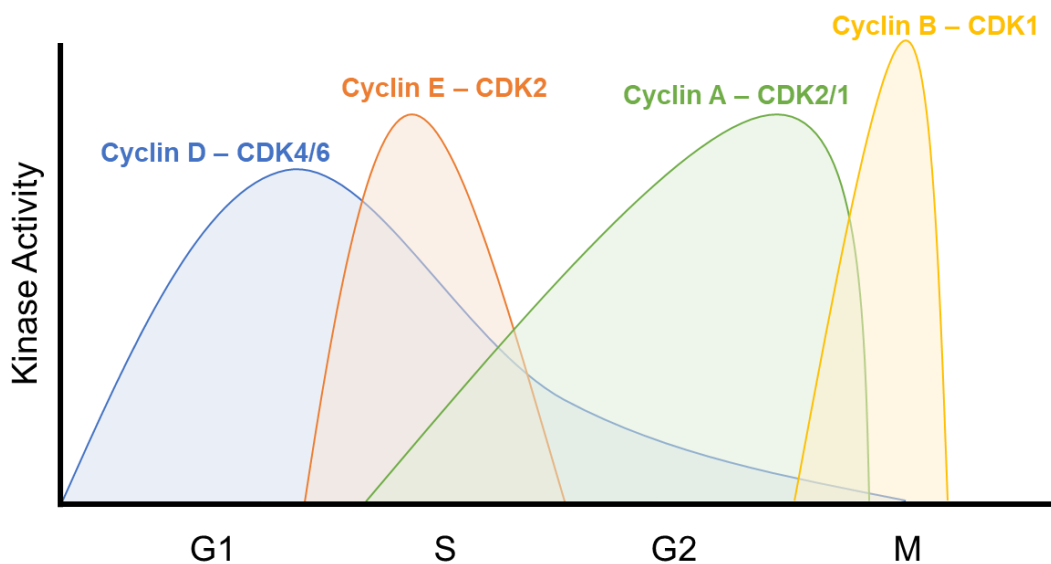


**Figure 1.2: Cyclin-CDK control of the cell cycle.** Cyclin D is expressed and activates CDK4/6 in early G1 phase (blue). Cyclin E is expressed and activates CDK2 in mid- G1 (orange), raising total kinase activity and driving cell entry to S phase. In late G1 – early S phase, Cyclin A is expressed which activates CDK2 and then CDK1 in G2 phase (green). In late G2 phase, cyclin B is expressed activating CDK1 (yellow), further increasing total kinase activity and driving cell entry to mitosis (Hochegger et al., 2008).

CIZ1 is an important part of the control and promotion of DNA replication. CIZ1 contacts pre-RC through direct Cdc6 interactions (Copeland et al., 2015). CIZ1 also interacts directly with cyclin A and cyclin E, coordinating their functions within the nucleus. CIZ1 interacts with cyclin

E in mid G1 phase and is displaced by cyclin A at the G1 – S transition, helping to ensure that they execute their functions in the replication initiation process sequentially in the same place (Copeland et al., 2010). This does not occur when CIZ1 is either mutated or depleted via siRNA (Copeland et al., 2010). Taken together, this supports the proposal that CIZ1 contributes to the delivery of cyclin-CDK2 complexes to the origins of replication (Copeland et al., 2015).

CIZ1 is also a CDK sensor that promotes initiation of DNA replication and prevention of re-replication (Copeland et al., 2015). Promotion of initiation of DNA replication occurs at low kinase levels, when in a hypophosphorylated state that is permissive for cyclin A–CDK2 interaction and delivery to licensed origins, whereas delivery to licensed origins is blocked at higher kinase levels when CIZ1 is phosphorylated (Copeland et al., 2015). Phosphomimetic mutations within CIZ1 prevent cyclin A-CDK2 binding and its replicative function (Copeland et al., 2015).

### **1.3.3 Role of CIZ1 in tumorigenesis**

Deregulation of CIZ1 expression, splicing and activity has been implicated in different cancer types, including four of the most common: breast, prostate, colorectal and lung cancers that constitute >50% of cancer incidence in the UK. The main mechanisms that studies have shown CIZ1 are involved are overexpression, regulation of transcription and alternative splicing.

CIZ1 promotes cellular proliferation in vivo and in vitro; (Copeland et al., 2010, Copeland et al., 2015) and can induce tumour formation in mouse xenograft models (Higgins et al., 2012), suggesting that CIZ1 can facilitate tumour growth. CIZ1 enhanced tumorigenesis in a number of tumours including breast (den Hollander et al., 2006), colorectal (Yin et al., 2013, Wang et al., 2014), hepatocellular carcinoma (Wu et al., 2016), gall bladder (Zhang et al., 2015), prostate (Liu et al., 2015), small cell lung and non-small cell lung carcinoma (Higgins et al.,

2012). In each case, CIZ1 has been implicated directly in tumour growth due to overexpression or alternative splicing (Higgins et al., 2012, Swarts et al., 2018). CIZ1 also has potential for a tumour suppressor role. Deletion of CIZ1 has no defects on murine development, but results in an increased risk of viral transformation and tumour growth (Nishibe et al., 2013) and increased risk of lymphoblastic tumours in aged mice (Ridings-Figueroa et al., 2017).

CIZ1 displays oncogene like functions when overexpressed. Increased CIZ1 expression promotes tumour growth and migration. One example of this is overexpression of CIZ1 in breast cancer, where CIZ1 aids recruitment of the oestrogen receptor (ER) complex to the target gene, resulting in enhanced ER transactivation activity. Subsequently, CIZ1 confers oestrogen hypersensitivity, therefore resulting in an increased rate of cellular proliferation (den Hollander et al., 2006). Additionally, CIZ1 overexpression has shown to promote tumour growth both in vivo and in vitro in hepatocellular carcinoma (HCC) cells. CIZ1 interacts with transcriptional factor Yes associated protein (YAP), positively regulating the YAP/Tafazzin (TAZ) signalling pathway. Overexpression of CIZ1 lead to an increased interaction between YAP/Transcriptional enhancer factor TEF (TEAD) and increased signalling of YAP/TAZ transcription factors, which in turn promoted growth and migration of HCC cells via increased expression of cyclin E and connective tissue growth factor (CTGF) (Wu et al., 2016, Lei et al., 2016).

A CIZ1 splice variant (b-variant), with alternative splicing between exon 14 and 15, was identified in small cell and non-small cell lung cancers. This variant is restricted to the tumour cells, and shRNA that reduces its expression resulted in a reduction in tumour size in xenograft models, making it an excellent potential biomarker candidate for lung cancer (Higgins et al., 2012, Coverley et al., 2017). Additionally, the alternative splicing of CIZ1 in exons 8-12 has been identified in early-stage solid tumours of breast and colon cancers (Swarts et al., 2018). Alternative splicing of exon 4 in Ewing tumour was found to influence the spatial distribution

of the CIZ1 protein within the nucleus, which raises the possibility that CIZ1 alternative splicing could influence organised patterns of DNA replication (Rahman et al., 2010, Rahman et al., 2007). The precise role of each splice variant has yet to be determined, but they may influence CIZ1 function or stability contributing to tumorigenesis.

## **1.4 Aims**

There is a direct link between CIZ1 overexpression in multiple tumour types. The aim of the current work is to investigate whether CIZ1 is detectable and/or differentially expressed in glioblastoma. In addition, this project will assess if CIZ1 expression is required for proliferation in neurological tumours. The work will be separated into 2 parts. The first will assess the viability of CIZ1 as a biomarker using FFPE glioblastoma tumours to determine CIZ1 staining pattern and localisation, comparing healthy and tumour areas. In addition, primary glioblastoma cell line BTNW914 will be compared with U87MG and a glial cell line SVGp12 to compare CIZ1 localisation in vitro. The second goal is to establish if CIZ1 contributes to glioblastoma proliferation by establishing transfection procedures to deplete CIZ1 using siRNA. Finally, the pharmacological reduction of CIZ1 levels through the inhibition of CDK or DDK kinases will be evaluated.

## **Chapter 2: Methods and Materials**

## 2.1 Cell Culture

SW620 (colorectal cell line) and U87MG (glioblastoma cell line) cells were cultured using Dulbecco's modified eagle medium (1 g/l glucose, with pyruvate and GlutaMAX I™) (DMEM) (GIBCO). SVGp12 cells (transformed glial cell line) were cultured using Eagle's minimal essential medium (EMEM) (Lonza). BTNW914 primary glioblastoma cells were cultured using F10 Ham's media. All media were supplemented with 1 % v/v penicillin, streptomycin, glutamine (100 X) (GIBCO) and 10 % (v/v) foetal bovine serum (FBS) (Labtech). Cells were grown in 15 cm diameter dishes in 30 ml of media or 10 cm diameter dishes with 10 ml media. Cells were incubated in a ThermoFisher Scientific Heracell™ 150i, at 37 °C in 5 % CO<sub>2</sub>. Cells were passaged every 2-3 days and maintained at 70% confluency. Media was discarded from cells and cells were rinsed in 10 ml Dulbecco's PBS (GIBCO), then trypsinised in 9 ml DPBS supplemented with 1 ml 0.5% trypsin-EDTA (GIBCO) for 2-3 minutes until cells were released from the plates. To protect cells, trypsin was neutralised with an equal volume DMEM and split evenly across the desired number of plates and made up to 30 ml with media.

## 2.2 Primary Cells

Primary glioblastoma cell lines from the Brain Tumour North West biobank (BTNW914, female, aged 67, glioblastoma patient) were established from human glioma biopsies obtained from the Brain Tumour North-West (BTNW) tissue bank at Royal Preston Hospital. Cells were maintained as described (Section 2.1).

## 2.3 Antibodies

A full list of antibodies used in this study are in Table 2.1. Monoclonal antibodies against actin (AC15, Sigma Aldrich), and polyclonal antibodies against, histone H3 (Abcam, ab1791) were used as directed for Western blotting and/or immunofluorescence. CIZ1 was detected with a rabbit polyclonal antibody raised against purified bacterially expressed recombinant ECIZ1-

N471 for this study (Covalab) (Pauzaite, 2019). For Western blots, goat anti-mouse-IgG conjugated to peroxidase (POD) (Sigma Aldrich) and goat anti-rabbit-IgG–POD (Sigma Aldrich) were used with an ECL detection system (GE Lifescience). For immunofluorescence, Alexa-Fluor®-488-conjugated goat anti-mouse-IgG (H+L) (A10667) (Invitrogen) were used. Phosphospecific anti-CIZ1 phospho-T293 (anti-pT293) was produced by immunisation of rabbits with TAPKQTQTpTPDRL peptide, where pT indicates phosphothreonine (Copeland 2015 Covalabs). Antibodies were purified by sequential subtraction on unphosphorylated peptide columns and enrichment on a phosphopeptide column, to purify phosphospecific anti-CIZ1 antibodies (Pauzaite, 2019).

Antibody	Supplier	Code	Dilution	Antibody	Conjugate
β-Actin	Sigma Aldrich	A-1978	1/5000	Mouse	N/A
Histone H3	Abcam	ab1791	1/10000	Rabbit	N/A
MCM2 (BM28)	BD	610700	1/500	Mouse	N/A
CIZ1	Covalabs	Copeland et al. 2015	1/1000	Rabbit	
pCIZ1 - T293	Covalabs	Copeland et al. 2015	1/250	Rabbit	
pMCM2-ser53 A300-756A	Bethyl Laboratories	A700-108	1/500	Rabbit	
Goat anti- Mouse IgG- HRP	Sigma Aldrich	A4416	1/5000	Goat	HRP
Goat anti- Rabbit IgG- HRP	Abcam	Ab7051	1/5000	Goat	HRP

**Table 2.1: Antibodies used in this study.** Supplier details, concentration used, species used, and conjugate indicated.

## **2.4 Sodium Dodecyl Sulphate Polyacrylamide Gel Electrophoresis (SDS-PAGE)**

Protein fractions were analysed by resuspension of cell fraction at a 1 in 4 ratio 4x SDS PAGE loading buffer (200 mM tris HCl pH 6.8, 27.7 mM SDS, 40% (v/v) glycerol, 1 mM DTT) and boiled for 10 minutes. Samples were loaded onto hand poured 10 % SDS-PAGE gels using the Mini-PROTEAN Tetra Cell System (BioRad) in Tris glycine SDS solution (TGS) (250 mM tris, 1.92 M glycine, 1% (w/v) SDS) between 100 V and 200 V for 1 hour. Gels were analysed by Western blotting.

## **2.5 Western Blotting**

After SDS-PAGE gels were soaked in transfer buffer (composition). Protein was transferred onto an Amersham Protran 0.45 nitro-cellulose membrane (GE Life Sciences) or polyvinylidene fluoride (PVDF) membrane (GE Life Sciences) using a semi dry transfer system. Filter paper, nitrocellulose/PVDF membrane and gels were all soaked in transfer buffer (750  $\mu$ M tris base (SIGMA), 10  $\mu$ M CAPS (SIGMA), 0.01% (w/v) SDS, 10% (v/v) ethanol (Fisher)). Four layers of filter paper were stacked, followed by the nitrocellulose/ transfer membrane, gel and then four more layers of filter paper. Protein was transferred at 1 mA/cm<sup>2</sup> of membrane for one and a half to two hours. Membranes were blocked in 10 ml blocking buffer (1% (w/v) BSA (Biowest), 0.05 M Tris, 0.138 M NaCl, 0.0027 M KCl, pH 8.0, 0.1% (v/v) TWEEN 20 (Sigma Aldrich)) for one hour. Membranes were incubated with specific primary antibody (Table 2.1) overnight at 4 °C. Blots were washed four times for five minutes in 5 ml blocking buffer. Blots were incubated with secondary antibody for one hour. Blots were washed four times for 5 minutes in 5 ml washing buffer (0.05 M tris, 0.138 M NaCl, 0.0027 M KCl, pH 8.0, 0.1% (v/v) TWEEN 20) prior to imaging. Blots were developed using the BIO-RAD ChemiDoc™ MP system.

## **2.6 Standardising Protein Loads**

Protein loads were standardised using actin or histone H3 load using quantitation of band intensities using the BIO-RAD Image Lab Software. 5 µl of sample was ran on SDS-PAGE and transferred to a nitrocellulose membrane. Membranes were probed for their load control and developed. Loading was adjusted across samples to ensure uniform load control band intensity. The band intensity was converted into relative number by dividing the protein band number by the actin band number to give relative quantity. The control was then equalised to 1 and every sample was divided by the relative control number showing relative variation from control.

## **2.7 Drug treatments**

Asynchronous cell populations at 50-70% in confluency, were treated with small molecule CDK2, CDK4/6 or DDK inhibitors as indicated (Table 2.2) either 7 hours or 24 hours prior to cell harvesting. These timepoints were selected to represent an acute and long timepoint, with the acute 7 hour timepoint capturing cells in different phases of the cell cycle, and the 24 hour timepoint allowing observation after a full cell cycle.

Drug	Target	Concentration	Provider
Palbociclib (PD0332991) Isethionate	CDK4/CDK6	10 $\mu$ M	Sigma Aldrich
PHA-767491 dihydrochloride	Cdc7	10 $\mu$ M	Sigma Aldrich
XL-413 hydrochloride	Cdc7	10 $\mu$ M	Selleckchem
Roscovitine	CDK2	30 $\mu$ M	Sigma Aldrich; Selleckchem
CVT-313	CDK2	10 $\mu$ M	Santa Cruz Biotechnology

**Table 2.2: Small molecule kinase inhibitors used in this study.** Small molecule, supplier, concentration and provider is listed.

## 2.8 Flow Cytometry

Cells were pulse labelled with EdU one hour prior to harvest. Cells were harvested by trypsinisation followed by centrifugation at 500 x g. EdU labelled cell pellets were washed (with centrifugation between each step for 5 min, 500 x g). 3 x with 500  $\mu$ l 1 % BSA in 1 x PBS, fixed with 4% PFA for 15 min, washed 3 x with 1% BSA, permeabilised with 0.5% Triton X-100 for 20 minutes, and washed 2 x with 1% BSA. Cells were protected from light and incubated for 30 minutes on ice with Click-iT™ EdU Cell Proliferation Assay Cocktail (Invitrogen) containing Alexa Fluor 488 or Alexa Fluor 566. Cells were washed 2 x with 1% BSA and 1 x with PBS and stained with 100  $\mu$ g/ml of Propidium Iodide in 0.1% Triton X-100 in PBS. Cells were analysed with Beckman Coulter CytoFLEX using FITC (525/40) and PE (585/42) channels. Data were collected for ~10,000 cells with consistent gating applied for all samples.

## **2.9 Determination of Percentage S-phase Cells by Ethynyl Deoxyuridine (EdU) Incorporation**

An hour before harvesting, cells were pulse labelled with 1  $\mu$ M EdU (Invitrogen). Cells were fluorescently labelled using the protocol outlined in the click-iT<sup>®</sup> EdU imaging kits protocol (Invitrogen). Coverslips were mounted in Vectashield with DAPI (Vector Laboratories). Percentage of cells in S phase was calculated using a Zeiss LED illuminated microscope and counting the fraction of DAPI labelled nuclei that had fluorescently labelled replication foci (alexafuor-488). Only nuclei with replication foci that were present throughout the nuclei were scored positive. Percentage of cells in S phase cells was calculated using Microsoft Excel to calculate percent positive for each experiment.

## **2.10 Nucleofection of cell lines**

Depletion of cells lines was performed using the Nucleofector<sup>™</sup> 2b system (Lonza). BTNW914 were transfected with anti-CIZ1 siRNA (s24489) in Cell Line Nucleofector<sup>®</sup> Solution for Primary Mammalian Glial Cells (Amaxa<sup>®</sup> Basic Nucleofector<sup>®</sup> Kit for Primary Mammalian Glial Cells; Lonza protocol). Nucleofector<sup>®</sup> programs A-033, E-013, G-013, O-017 and T-020 were selected for transfection optimisation according to manufacturer's optimisation protocol using GFP, then program T-020 was used thereafter following transfection optimisation. The composition of the transfection reagent and current/voltage settings are proprietary and are not freely available. The cells were harvested after 24 hours for protein and RNA analysis, and 24, 48, and 72 hours for flow cytometry analysis as indicated in the figures.

## **2.11 RNA extraction and qPCR**

Cells were harvested and their total RNA was purified using PureLink<sup>®</sup> RNA Mini Kit (Invitrogen) according to providers instructions. RNA was first quantified using Nanodrop (ThermoScientific). Then quantitation of transcript abundance was performed using SuperScript<sup>™</sup> III Platinum<sup>™</sup>

One-Step qRT-PCR Kit (Invitrogen) using 25 ng of total RNA and primers for CIZ1 (Hs00967155) and GAPDH (Hs02758991) using a FX96 Touch™ Real-Time PCR Detection System (BIO-Rad). Program used: 42–60°C, 95°C for 2 minutes hold, 40 cycles of 95°C - 15 seconds, 60°C - 30 seconds. Relative expression was calculated as a mean fold change of the difference between control gene ct and the gene of interest ct,(delta ct) then all results divided by control results.

## **2.12 Sub-Cellular Fractionation**

Cells were scrape harvested, and cell debris volume determined. All steps were performed on ice. The total volume was made up to an equivalent volume for all samples in PBS, 1mM EDTA, 1x complete protease inhibitor cocktail (Roche) and 1 mM DTT. Half of the sample was immediately taken as the total protein fraction. The remaining half was centrifuged at 5000 x g for 5 minutes. The resulting supernatant was the cytosolic/nucleosolic fraction and pellet was chromatin fraction. All fractions were resuspended in a 1 in 4 ratio 4x SDS PAGE loading buffer (200 mM tris HCl pH 6.8, 27.7 mM SDS, 40% (v/v) glycerol, 1 mM DTT). Samples were stored at -20 °C until use.

## **2.13 Immunohistochemistry of BTNW patient samples**

Formalin fixed paraffin embedded (FFPE) tumour sections were provided by Preston Royal Hospital. Patient samples provided had been prepared to the point of paraffin removal. These samples include: BTNW2265, BTNW2803, BTNW2819, BTNW2424, BTNW2422 and BTNW2430.

### **2.13.1 Antigen Retrieval**

Sections were dewaxed in xylene, taken to absolute alcohol, then washed under running tap. A pressure cooker was filled with 1.5L of 0.01 M citrate buffer pH 6.0 (0.02 M Citric Acid

Crystals, 0.05 M NaOH) and brought to boil inside the microwave, lid on but not fully closed. Slides placed in the heated buffer within the pressure cooker, fully sealing the lid. Heated in microwave until pressure cooker valve had risen. Once risen, heated for a further 2 minutes. Allowed pressure cooker to cool until valve had dropped. Slides were then removed and rinsed in warm tap water, gradually introducing more cold water for 10-15 minutes. Then proceeded with immunostaining.

### **2.13.2 Immunostaining using the Vectastain Elite Universal ABC Kit**

Immunostaining of tumour sections was conducted using the VECTASTAIN® Elite® ABC Universal Kit Peroxidase (VECTORLABS). Sections were washed under running tap water. Sections were rinsed with pH 7.4 TBS (500 ml of distilled water, 0.05 M Tris HCL, 0.079 M Sodium Chloride, 1% w/v Bovine Serum Albumin). Back of slide was dried and placed on immunostaining tray. Area around section was dried, and Dako hydrogen peroxide blocking reagent was placed on the sections for 5 minutes. Slides were drained and washed with TBS. Slide was dried around the tumour section. VECTASTAIN® Blocking Serum was added to sections for 20 minutes, then drained and dried. Primary antibody was placed on slides, and left overnight at 4°C. The following day, slides were washed in TBS, and incubated in VECTASTAIN® Biotinylated Universal Antibody for 30 minutes. Slides washed in TBS. Samples were then incubated VECTASTAIN® StreptABComplex/HRP Solution for 30 minutes, then washed in TBS. One drop of DAB chromogen was added to 1ml of Dako substrate buffer and placed on sections for 10 minutes. Slides were washed in running water, counterstained in haematoxylin for 5 seconds, then washed immediately in hot running water until water ran clear from blue staining. Slides then dehydrated in alcohol, soaked in xylene and mounted in styrolite.

## **2.14 Ethics Statement for use of Patient Samples and Primary Cells**

Ethical approval and informed consent was obtained by East of England - Cambridge East Research Ethics Committee for the use of human tissues to the Brain Tumour North West (BTNW) research bank (Approval reference no. 14/EE/1270). A confirmation letter was issued to the BTNW research bank stating the approval of participants written consent form for the collection of tumour and non-cancerous brain tissues for future use. The current study was approved by the Brain Tumour North West research committee for the use of tissue sections from 6 grade IV glioblastoma patients and BTNW914 primary cells.

**Chapter 3: Determination of CIZ1  
localisation and expression in  
glioblastoma**

### 3.1 Introduction

A biomarker should be specific and sensitive to the tumour type and be able to discriminate between healthy and diseased states. Biomarker specificity is the proportion of subjects without the target condition in whom the test result is negative, whereas biomarker sensitivity is the proportion of subjects with the target condition in whom the test result is positive (Mazzone et al., 2017). There are a handful of diagnostically useful biomarkers currently for glioblastoma, however, they lack both the sensitivity and specificity required. The most clinically relevant diagnostic biomarkers are IDH1/2 mutation, MGMT promoter methylation, and EGFR amplification/mutation (Szopa et al., 2017). IDH1/2 is mutated in almost all secondary glioblastomas, making it diagnostically relevant. The drawback being, only 10% of glioblastoma cases are secondary, making this biomarker ineffective at diagnosing 90% of cases. However, this selectivity provides prognostic information and can also guide treatment for this subgroup.

Methylated MGMT promoters are present in about 40% of glioblastoma cases and is used to distinguish true progression and pseudoprogression in patients with newly diagnosed glioblastoma (Szopa et al., 2017). This is also a useful prognostic marker as patients with MGMT promoter methylation have significantly improved response to the TMZ treatment. Again, this biomarker leaves 60% of cases undiagnosable. EGFR amplification is seen in approximately 40% of cases, and is often associated with high-grade tumours in the Classical subgroup (Verhaak et al., 2010). Additionally, approximately half of patients that present with EGFR amplification have a constitutively active mutation due to deletion of exons 2-7 (EGFRvIII) that is absent in patients without EGFR amplification. Prognostically, overall survival in patients with this EGFRvIII mutation is improved, particularly in combination with non-mutated PTEN, methylated MGMT promoter and <20% Ki64 levels (Szopa et al., 2017, Montano et al., 2011). Together, these biomarkers can build up a picture that can lead to a glioblastoma diagnosis and ruling out of other gliomas.

However, due to the lack of a specific biomarker in glioblastoma diagnosis, finding a biomarker that is able to distinguish between healthy and characteristic glioblastoma brain tissues would be of clinical significance.

## **3.2 Immunohistochemistry using polyclonal CIZ1 antibodies**

### **3.2.1 Antibody Optimisation**

Here, CIZ1 levels are determined in FFPE glioblastoma tumours from the BTNW biobank. The optimisation of a novel polyclonal anti-CIZ1 antibody is used to stain sections. Expression, localisation and cell types that are stained are determined. Initially, an antibody titration was performed to determine the optimum concentration of CIZ1-N471 immunopurified antibody to use, that would allow observation of CIZ1 staining without non-specific background staining. Sections were prepared by staff at Preston Royal Hospital to the point of paraffin removal. From here, antigen retrieval and immunostaining were undertaken to label sections with CIZ1-N471 immunopurified antibody, stained with DAB and counterstained with haematoxylin. CIZ1 antibody concentrations used ranged from 1:50 to 1:800 using patient sample BTNW2803. Two images taken at each concentration: one from a non-tumour section (left column) and the other from a section at the intersection of tumour and non-tumour (right column) (Figure 3.1). The left column clearly shows a reduction in the brown DAB stain as the antibody concentration reduces, whereas the right column shows the DAB stain reduces in healthy tissue but remains in the tumour demonstrating antibody selectivity and specificity. From these results, the staining seen at the 1:800 concentration of CIZ1 antibody shows the highest degree of specific staining, with minimal background stain. Therefore, this concentration was used to label all subsequent sections.

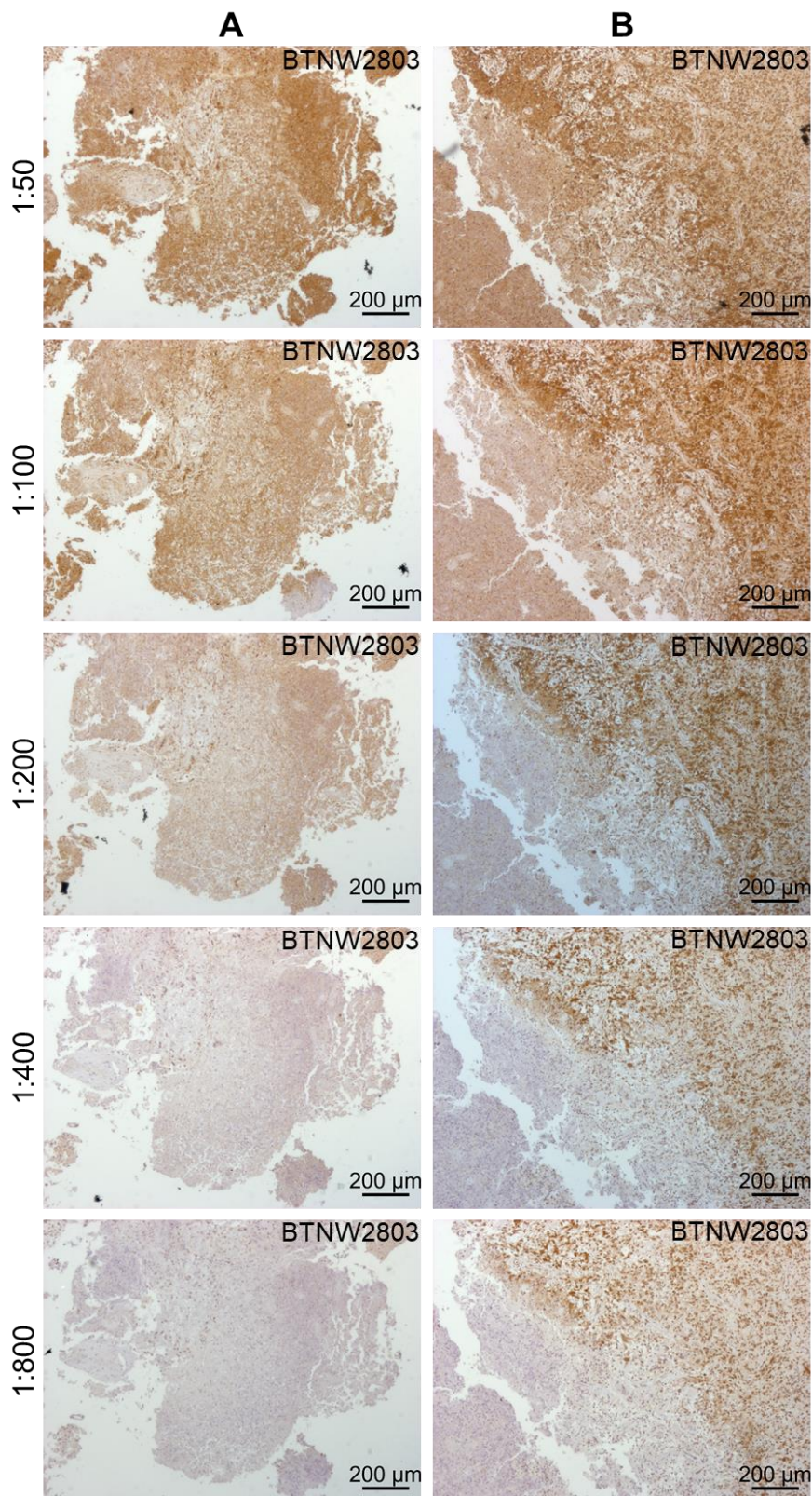


**Figure 3.1: Optimisation of CIZ1 antibody for immunohistochemistry.** Glioblastoma patient sample BTNW2803. CIZ1 dilutions of 1:50-1:800 were used. **A.** Images taken of normal cortex. **B.** Images taken at an intersection between tumour and non-tumour tissue. DAB stained (brown) with haematoxylin counterstain of nuclei (blue). Scale bars are shown by black bars in bottom right of image.

### 3.2.2 Observed CIZ1 staining in normal tissues is limited to specific cell types

In order to identify the CIZ1 staining patterns seen within tumour sections, the staining patterns seen within the normal tissue sections that surround the tumour areas were analysed. Firstly, we looked within the cortex of the samples and observed CIZ1 staining in neuronal cells (Figure 3.2). In each case, the cells' projected axons are facing towards the brain surface. Interestingly, the neurons in these patient samples stained with CIZ1 both in the cytoplasm and nucleus. Notably, oligodendrocytes are not efficiently stained, as a single oligodendrocyte can extend its processes to 50 axons, therefore would be visible spanning across neurones. This would suggest that CIZ1 levels are low in this cell type.

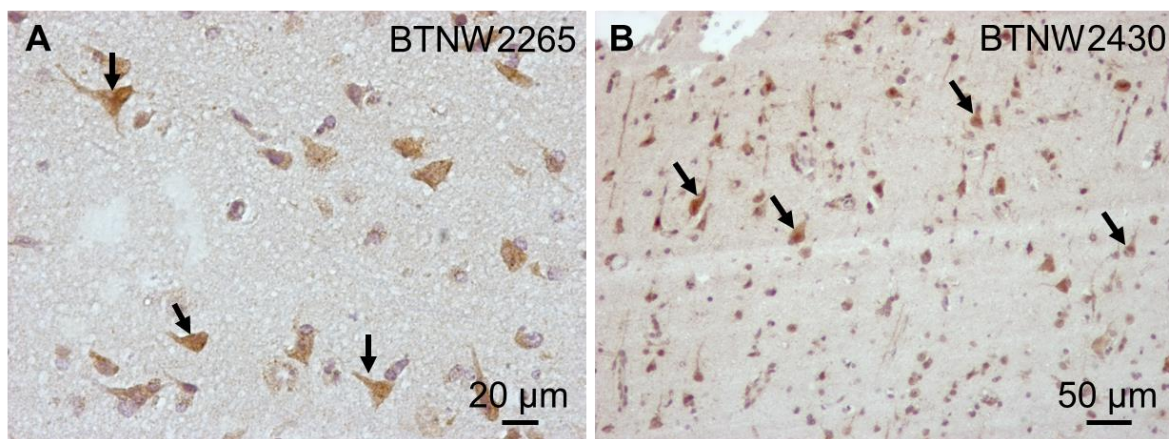


**Figure 3.2: CIZ1 staining of neurons in healthy tissue.** Black arrows pointing out examples of neurons being stained positively for CIZ1. Neural axons point towards cortex surface. DAB stained (brown) with haematoxylin counterstain of nuclei (blue). Scale bars are shown by black bars in bottom right of image. **A.** Image of neurons within healthy cortex of patient sample BTNW2265. **B.** Image of stained neurons near healthy cortex surface of patient sample BTNW2430.

There was also consistent staining of endothelial cells. From the patient samples, it appears that endothelial CIZ1 staining occurs exclusively in the tumour region, whereas no CIZ1 staining is seen in the endothelial cells in the normal tissue areas (Figure 3.3). Although the tumours sections imaged here show this relationship, it remains to be determined that this is a consistent feature for CIZ1 staining across a larger sample size of patients.

This observation could be explained by the production of VEGF by growing tumours, reported widely. Glioblastoma is characterised by increased vascularisation due to tumour induced angiogenesis by localised over overproduction of VEGF in the tumour (Linkous and Yazlovitskaya, 2011). As CIZ1 has a role in the efficiency of DNA replication and its expression increases through the cell cycle, this increased staining may reflect a more proliferative phenotype for endothelial cells and tumour cells.

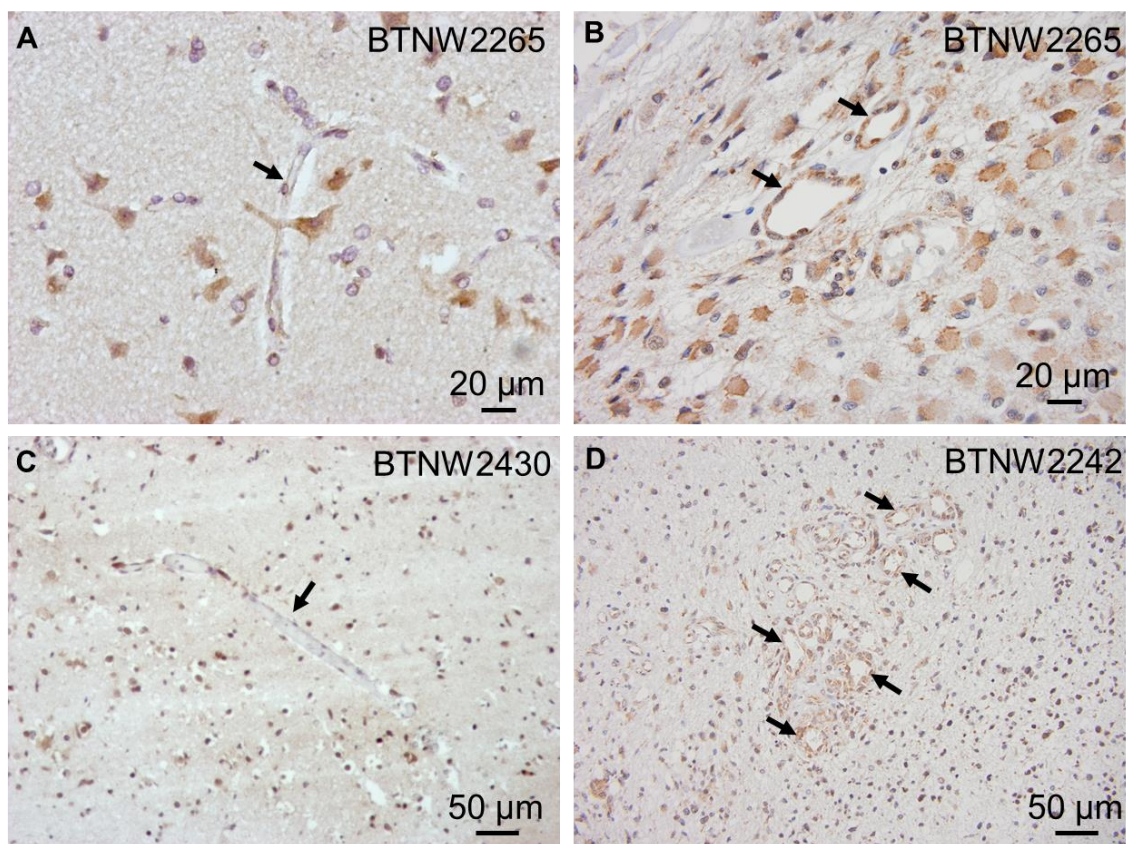


**Figure 3.3: Differential staining of endothelial cells.** Sections were DAB stained (brown) with haematoxylin counterstain of nuclei (blue) from 3 patients as indicated. Black arrows indicate endothelial cells and scale bars are shown by black bars in bottom right of image. **A+C.** Endothelial cells without CIZ1 staining within a non-tumour area. **B+D.** Numerous endothelial cells within a tumour area all positively stained for CIZ1.

### 3.2.3 Basic cancer morphology

Next, to observe CIZ1 expression and localisation within tumour samples, 6 patient samples were imaged. A common observation between the patient samples was the consistent staining

within gemistocytes. Gemistocytes are a type of GFAP expressing astrocyte, which in response to a stressor, has retracted its processes and has swollen to become globose in shape, resulting in the nucleus being pushed to the edge of the cell (Avninder et al., 2006). Figure 3.4 shows examples of these gemistocytic astrocytes, some of which are indicated by black arrows. Significantly, there is clear CIZ1 staining within the cytoplasm, that is uncommon in tissues where immunofluorescence has been used to determine subcellular localisation, where CIZ1 is predominantly nuclear even when overexpressed with a GFP reporter (Ainscough et al., 2007, Coverley et al., 2005). However, within the tumour there is an increase in cytoplasmic CIZ1 stain, and the functional consequences associated with the mislocalisation has not been determined.

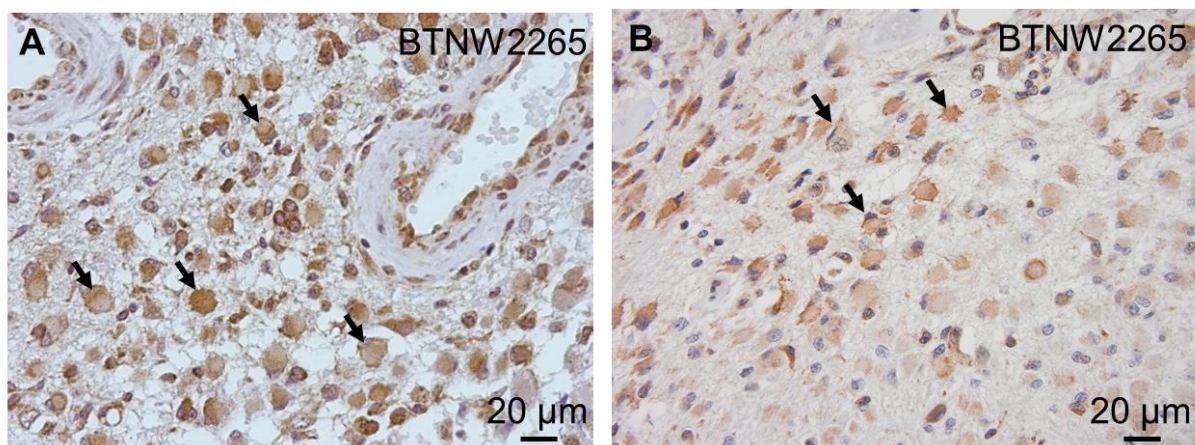


**Figure 3.4: CIZ1 staining of gemistocytic astrocytes.** Black arrows indicate gemistocytes, globose in shape with nucleus pushed to edge and retracted processes. DAB stained (brown) with haematoxylin counterstain of nuclei (blue). Scale bars are shown by black bars in bottom right of image. **A.** Image of tumour section of cortex, highlighting staining of gemistocytic astrocytes of patient sample BTNW2265 where both nucleus and cytoplasm are stained. **B.** Image of tumour section of cortex, highlighting staining of gemistocytic astrocytes of patient sample BTNW2265 demonstrating cells where only cytoplasm is stained.

Oedema is another common characteristic of cancer and predicts poor clinical outcome in glioblastoma (Wu et al., 2015). High amounts of oedema were found within tumour sections of different patient samples (Figure 3.5).

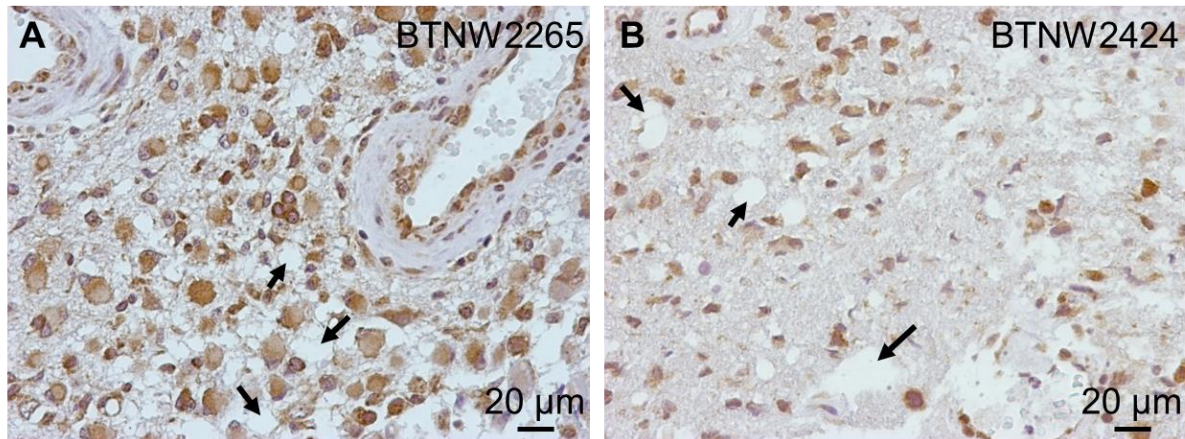


**Figure 3.5: Oedema within tumour section.** Oedema indicated by black arrows and scale bars shown with black bars. DAB stained (brown) with haematoxylin counterstain of nuclei (blue). Scale bars are shown by black bars in bottom right of image. **A.** Image of oedema within tumour section of cortex of patient sample BTNW2265. **B.** Image of oedema within tumour section of cortex of patient sample BTNW2424.

Centrosome amplification occurs frequently in almost all types of cancer, and is considered as the major contributing factor for chromosome instability in cancer cells (Fukasawa, 2005). Healthy cells normally have two centrosomes, which allows the usual bipolar segregation of chromosomes along a single plane during mitosis. The production of multiple centrosomes in some cancer cells can result in a multipolar segregation, leading to the production of either non-viable cells or aneuploid cells (Fukasawa, 2005, Bose and Dalal, 2019). Figure 3.6 shows at least two examples of this multipolar segregation (black arrows) that is characterised by loss of chromosomal organisation along a single plane, with chromosomes being pulled in 3 or more planes. However, whilst these cells do show DNA staining reminiscent of multipolar mitoses, the cells themselves are so large they are almost certainly a different cell type to most cells in this image. The size and appearance of the cells suggest possible immune infiltration. The presence of immune infiltrate in gliomas is common, but it is still in debate as to whether this affects prognosis positively or negatively, and may be dependent on different immune cell microenvironments (Domingues et al., 2016). Figure 3.6 has also captured numerous mitoses taking place, another characteristic of cancer, representing the rapid and uncontrolled division that occurs in cancer.

Mitosis is usually underrepresented in paraffin sections, therefore observing numerous mitoses in one field of view demonstrates the aggressive nature of this cancer.

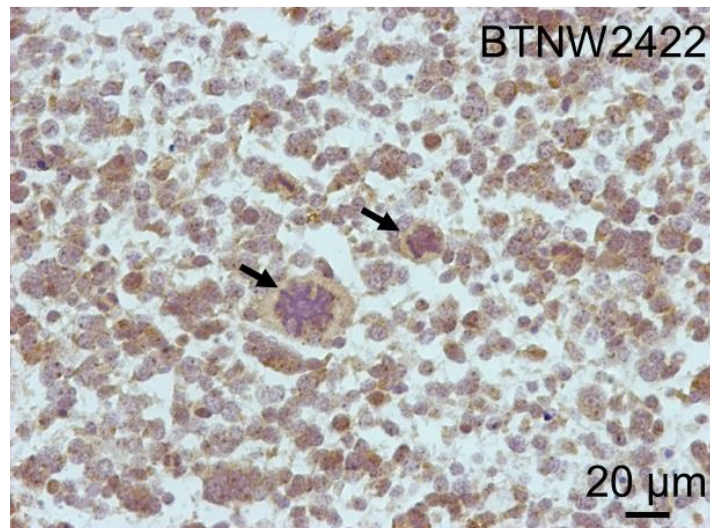


**Figure 3.6: Multipolar cells are characteristic of glioblastoma.** Black arrows indicate multipolar cells, where the nuclei are in the process of a multidirectional mitosis. DAB stained (brown) with haematoxylin counterstain of nuclei (blue). Scale bars are shown by black bars in bottom right of image.

### 3.2.4 CIZ1 overexpression and specificity in patient IHC samples

Having established parameters for anti-CIZ1 IHC, the next aim was to determine whether the CIZ1 staining was selective for tumour cells over healthy cells. Six glioblastoma FFPE patient tumour samples were used and labelled with CIZ1-N471 immunopurified antibody, stained with DAB and counterstained with haematoxylin. This revealed that CIZ1 was expressed at higher levels within the tumour and there is a clear quantitative difference in staining within and proximal to the tumour (Figure 3.7) that identifies the region where tumour cells meet normal brain that is demarcated by the red dashed line. Comparing each side of the demarcation for each image, there is a clear difference in both morphology and staining. The difference in morphology alone indicates a stark visual contrast, allowing us to have confidence that the highly stained area is in fact tumour. In addition, there is an increase in

CIZ1 staining, and increase in cell density in the tumour region, oedema and mis-localisation of CIZ1 protein to the cytoplasm. These features are common to each of the six patient sections, but the levels of CIZ1 expression are variable. These data suggest increased CIZ1 staining is tumour specific, suggesting that CIZ1 is overexpressed in glioblastoma tumour cells.

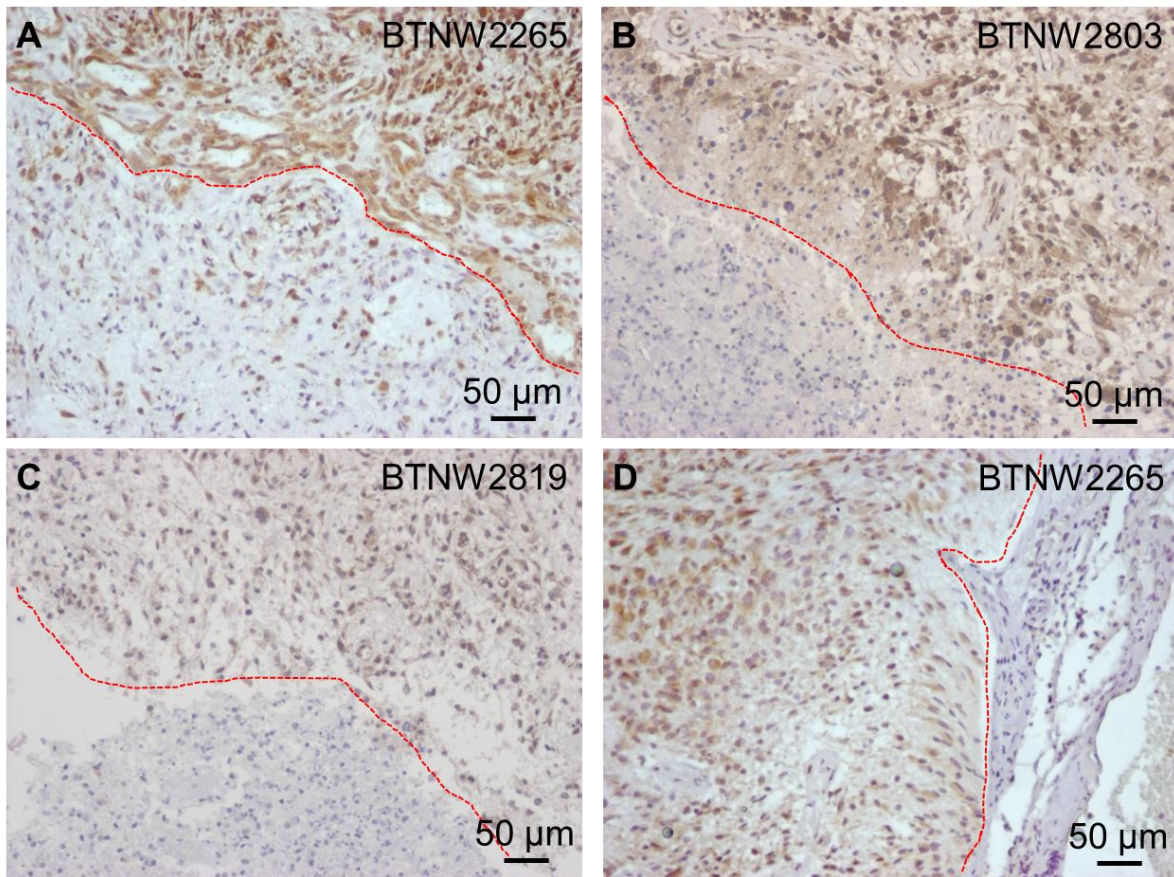


**Figure 3.7: Representative anti-CIZ1 IHC of FFPE sections.** Differential CIZ1 staining at tumour intersection. Red line shows the demarcation between normal and tumour tissue. DAB stained (brown) with haematoxylin counterstain of nuclei (blue). Scale bars are shown by black bars in bottom right of image. **A.** Intersection between healthy and tumour section of cortex of patient sample BTNW2265. **B.** Intersection between healthy and tumour section of cortex of patient sample BTNW2803. **C.** Intersection between healthy and tumour section of cortex of patient sample BTNW2819. **D.** Intersection between healthy and tumour section of cortex of patient sample BTNW2265.

### 3.2.5 Micrometastases and Invasion

Glioblastoma is a highly aggressive tumour type that migrates and invades surrounding and distal tissue. Here the migration of the tumour through brain tissue is observed and this visualisation is enhanced by the increased contrast provided by CIZ1 staining within glioblastoma. An example using BTNW2430 sample is shown in Figure 3.8, which shows an example of cancer cells migrating along the pia mater (red arrow). The brain surface is comprised of six distinct layers, with the pia mater being the innermost. A pia vessel, marked by the black arrow, is seen as an invagination from the pia mater layer, that shows increased CIZ1 staining in tumour cells invading normal cortex.

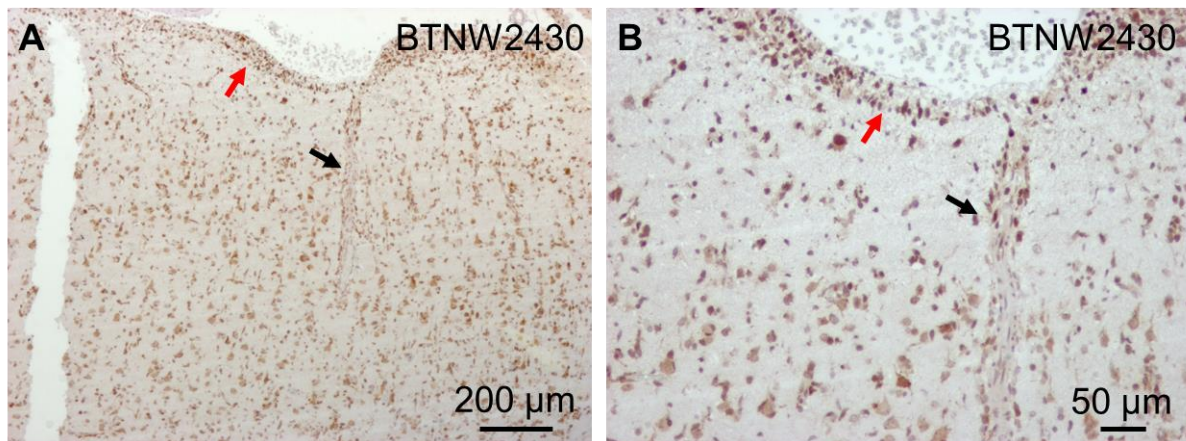


**Figure 3.8: Brain surface with pia vessel infiltrating from pia mater at two magnifications.** Red arrows indicate pia mater layer, black arrows indicate the infiltrating pia vessel. DAB stained (brown) with haematoxylin counterstain of nuclei (blue). Scale bars are shown by black bars in bottom right of image. **A.** Image of cortex and cortex surface, showing migration of tumour cells along pia mater, and infiltration of cells via pia vessel in patient sample BTWN2430. **B.** Higher resolution image of cortex and cortex surface, showing migration of tumour cells along pia mater, and infiltration of cells via pia vessel in patient sample BTWN2430.

In addition, there was evidence for the use of anti-CIZ1 IHC can aid in the visualisation of micrometastases. Micrometastases are a small collection of cancer cells from the original tumour that have spread to another part of the body through the blood or lymph nodes, or in some cases, a clonal variant within the tumour, typically less than 2 mm. The ability to identify small clusters of metastatic tumour cells would be significant, aiding in clinical staging and

gauging the aggressiveness of individuals tumour. Anti-CIZ1 IHC was able to identify micrometastases from 2 of 6 patients in this study further supporting the potential role for CIZ1 as a glioblastoma biomarker (Figure 3.9). Here, BTNW2430 shows a large cluster of cells that have metastasised from the primary tumour. Importantly, anti-CIZ1 IHC has also been able to identify small clusters <50 microns, suggesting that this may be a sensitive approach to visualise metastatic disease even in very small clusters (BTNW2819).

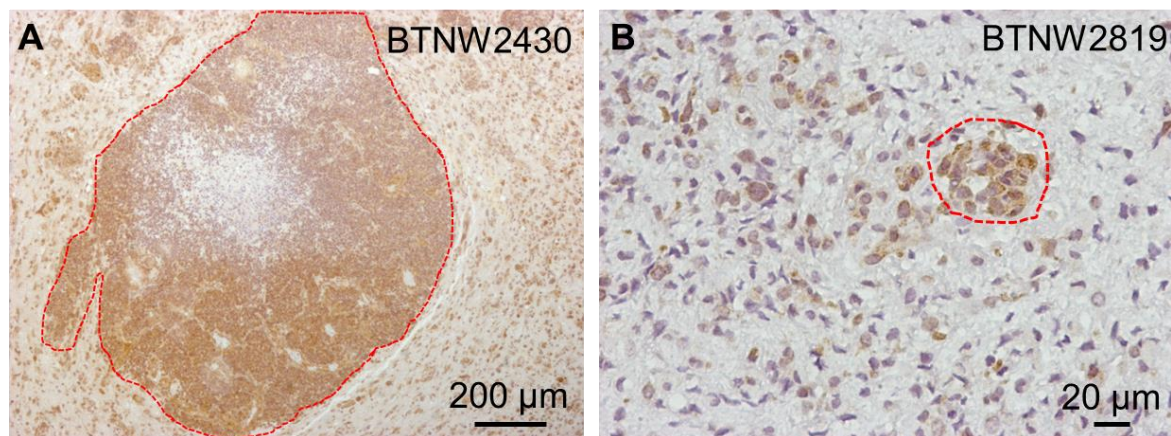


**Figure 3.9: Areas of tumour heterogeneity within a glioblastoma tumour area.** Area within the red line demarcation represents the clonal variant. DAB stained (brown) with haematoxylin counterstain of nuclei (blue). Scale bars are shown by black bars in bottom right of image. **A.** Macrometastasis of clonal variant within tumour section of brain cortex taken from patient sample BTNW2430. **B.** Micrometastasis of a small cluster of clonal variant cells within brain cortex taken from patient sample BTNW2819.

### 3.3 Localisation and expression of CIZ1 in neural cell lines

#### 3.3.1 Fractionation of neural cell lines

An unexpected observation from patient samples was the mis-localisation of CIZ1 to the cytoplasm of tumour cells in each of the 6 patient FFPE sections (Figure 3.4). CIZ1 is predominantly nuclear in murine and human cell lines, even when expressed ectopically (Ainscough et al., 2007, Copeland et al., 2010, Copeland et al., 2015, Coverley et al., 2005). This mislocalisation could be a feature of its deregulation in glioblastoma. To assess whether there are detectable changes in CIZ1 localisation, transformed glia (SVGp12), glioblastoma cell lines (U87MG) and primary BTNW914 glioblastoma cell lines were used. Cellular

fractionation was performed producing nuclear and cytoplasmic fractions to confirm whether what was observed in the brain tumour IHC samples would be recapitulated *in vitro*. Fractions from primary cell line BTNW914 were collected, alongside cell line U87MG and normal cell line control SVGp12. Unfortunately, it proved difficult to produce images with all fractions beside each other due to differing levels of proteins in each fraction, making it difficult to make direct comparisons. However, we were still able to compare CIZ1 levels within each cell type and its localisation. In SVGp12, BTNW914 and U87MG cell lines, CIZ1 is present in both the cytosolic and nuclear fractions, which is consistent with what was observed from the IHC patient glioblastoma sections. Consistently, the lower CIZ1 band from the nuclear fraction was missing or significantly reduced. Surprisingly, while the cytosolic CIZ1 fractions of the BTNW914 and SVGp12 exhibit a very similar pattern in the CIZ1 bands, the U87MG cell cytosolic fraction exhibits loss of the top band. The multiple bands seen may be due to a splice variation, which have been discovered in other cancers (Coverley et al., 2017, Rahman et al., 2010, Swarts et al., 2018), or possibly a post-translational modification (PTM). These data suggest that CIZ1 is localised both in the nucleus and the cytoplasm. The limitation of this approach is that we are unable to monitor cell to cell variation that can be determined using microscopy methods. In addition, permeabilisation of the nuclear membrane releases nucleosolic CIZ1 pools that may confound interpretation in cellular fractionation studies.

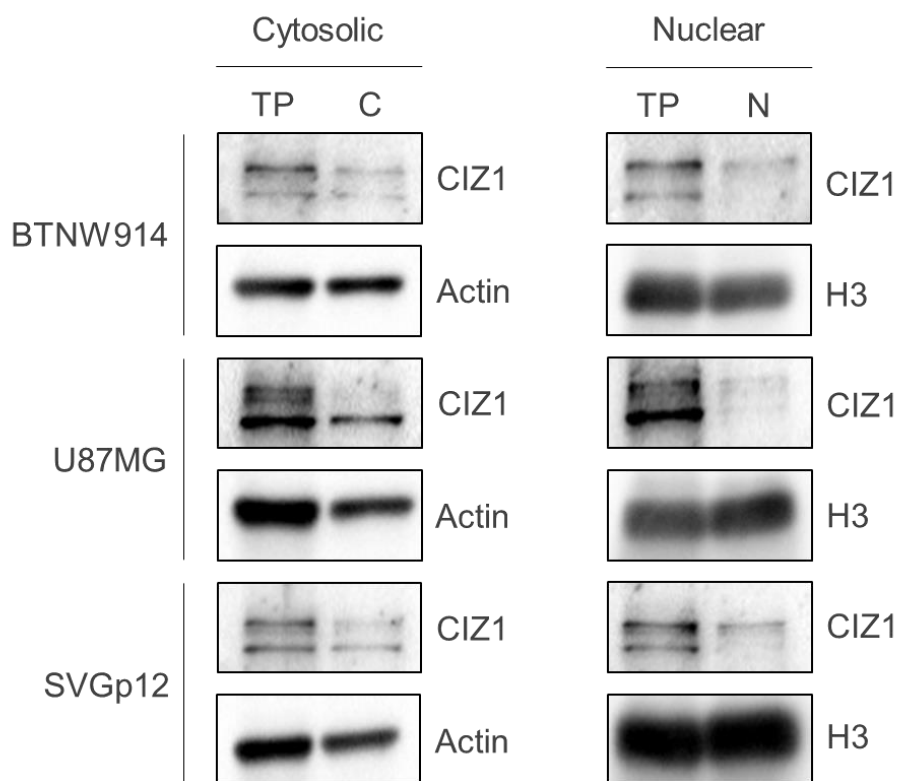


**Figure 3.10: Fractionation of neural cell lines.** BTNW914, U87MG and SVGp12 cells were split into fractions of total protein (TP) cytosolic (C) and nuclear (N). Western blot was probed for CIZ1 and Actin for cytosolic fraction and CIZ1 and H3 for nuclear fraction.

### 3.3.2 Immunofluorescence of neural cells

To complement the fractionation approach and to visualise CIZ1 expression and localisation within individual cells, immunofluorescence confocal microscopy was used. Initially, to determine the optimum CIZ1 antibody concentration in BTNW914 cells, 2-fold dilutions were performed, with concentrations ranging from 1:200 to 1:1600. Images were taken using an epifluorescence microscope using different filters to view either CIZ1 staining using Alexafluor-568, or nuclear staining using DAPI. With all concentrations used, cytoplasmic staining is visible, with the optimal anti-CIZ1 antibody dilution found to be 1:400 (Figure 3.5).

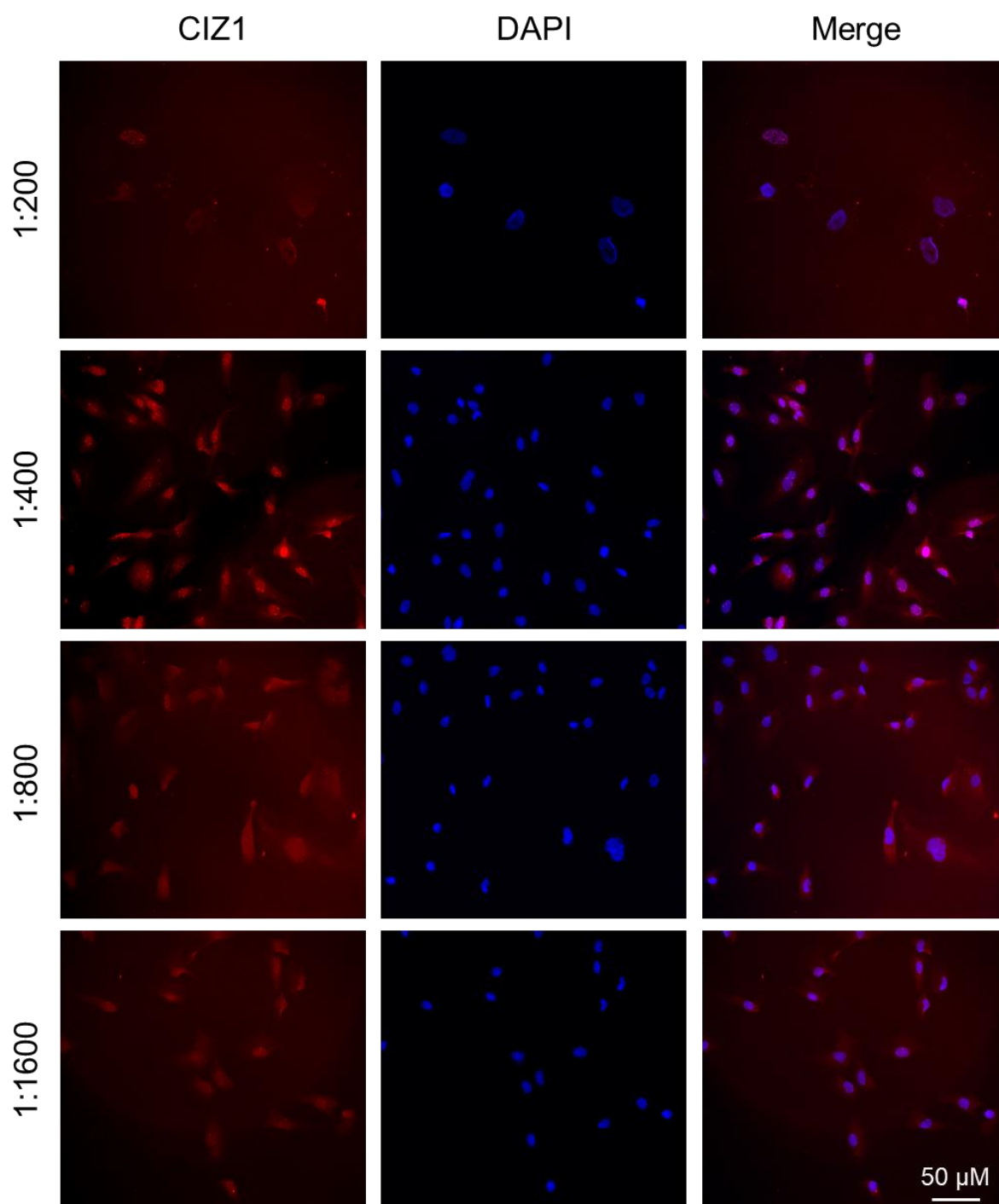


**Figure 3.11: Optimisation of CIZ1 antibody for immunofluorescence with BTNW914 cells.** Representative immunofluorescence images of BTNW914 cells treated with CIZ1 antibody dilutions of 1:200-1:1600.

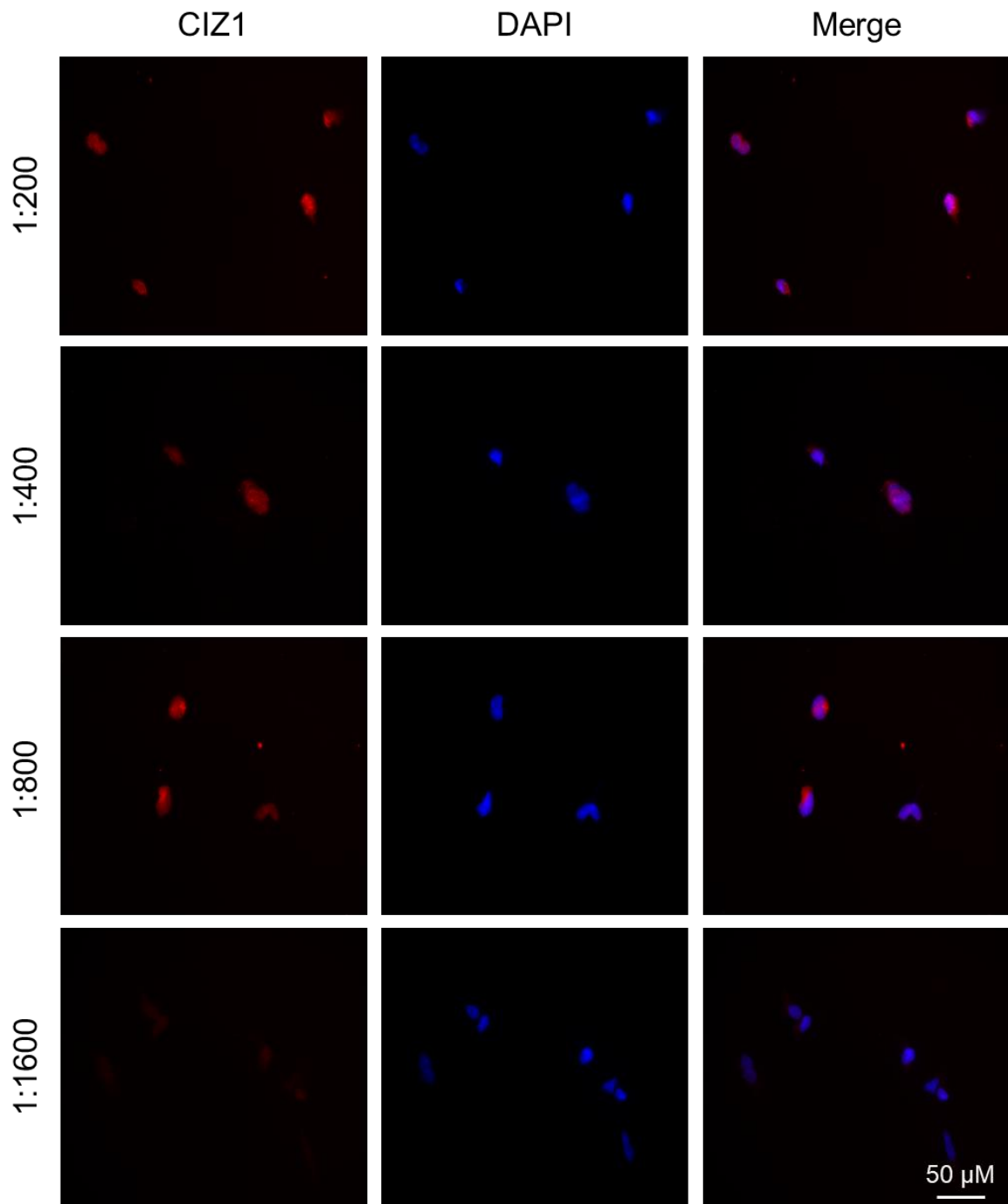


**Figure 3.12: Optimisation of CIZ1 antibody for immunofluorescence with SVGp12 cells.** Representative immunofluorescence images of cells treated with CIZ1 antibody dilutions of 1:200-1:1600.

Two CIZ1 foci appear frequently within the BTNW914 nuclei that were produced from a female patient. The large clusters of CIZ1 within the nucleus were reminiscent of CIZ1 localisation with the inactive X-chromosome and its role in X chromosome inactivation with Xist. One study

found a very similar staining pattern of CIZ1 foci within the nucleus, and determined the relationship between CIZ1 and Xist (Sunwoo et al., 2017).

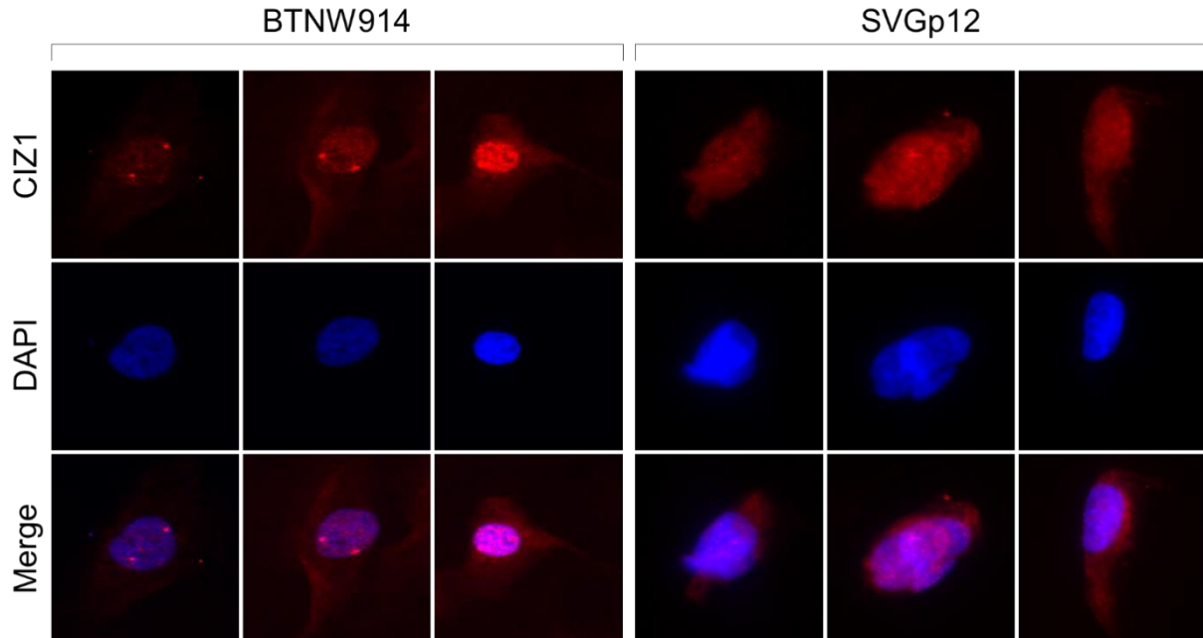


**Figure 3.13: Representative immunofluorescence images of BTNW914 and SVGp12 cells.** Representative immunofluorescence images of cells treated with CIZ1 antibody dilutions of 1:800.

Images of each cell type were taken at higher magnification to allow comparison (Figure 3.13). The images taken represent different observed CIZ1 expression patterns. The localisation of CIZ1 in 'normal' SVGp12 cells is both nuclear and cytosolic, all displaying similar patterns of expression. On the contrary, CIZ1 localisation patterns in BTNW914 differ from each other in these images. Varying levels of cytosolic expression is seen. The two foci seen in the BTNW914 cells previously are clear in two of the BTNW914 cells here. However, the cell in the third BTNW914 column displays an increased level of expression, with a more disperse distribution of foci, not the two distinct foci as seen in the other examples.

## 3.4 Chapter Discussion

### 3.4.1 CIZ1 appears be a biomarker for glioblastoma and identifies tumour margins and micrometastasis.

CIZ1 has been used as a biomarker in lung cancer (Higgins et al., 2012, Zhou et al., 2018). CIZ1 was used as circulating biomarker in patients with non-small cell lung cancer (Higgins et al., 2012, Coverley et al., 2017). For speed, ease and safety in the diagnostic processes, the use circulating biomarkers is beneficial as it only requires taking blood from a patient rather than a biopsy. However, the use of CIZ1 as an early circulating biomarker may not be viable in with glioblastoma due to the blood brain barrier. However, as the disease progresses, there may be detectable CIZ1 in serum after the blood brain barrier is disrupted through tumourigenesis.

One of the most important hallmarks of glioblastoma is tumour heterogeneity, from which the cancer's name originates. Not only does intertumoral heterogeneity exist between patients, such as what is seen in the aforementioned molecular subtypes (Verhaak et al., 2010, Friedmann-Morvinski, 2014), but also heterogeneity within the tumour of a single patient. Intratumoural heterogeneity is mostly characterised by distinct genetic alterations that occur in individual tumours originating in the same organ. Examples of intratumoural heterogeneity were found in some of our own IHC samples (Figure 3.9).

Within one patient sample, a relatively large area of tumour cells was strongly stained for CIZ1 (Figure 3.9). Even without CIZ1 staining, it would have been apparent in this case that this was a tumour metastasis by looking at the density and arrangement of cells. What is interesting is the differentially stained within the tumour area. The large group of highly stained tumour cells were amongst other tumour cells that were less stained (Figure 3.9). This indicates intratumoural heterogeneity, which in itself, poses a challenge in terms of treatment,

as it has been described as one of the root causes for therapy resistance (Saunders et al., 2012).

One study showed that at single cell RNA-sequencing resolution, a single tumour consisted of a heterogeneous mixture of cells representing all of the different glioblastoma subgroups (Patel et al., 2014). Another study showed that single cell derived glioblastoma subclones have distinct genetic identity and maintain differential drug resistance profile (Reinartz et al., 2017). Interestingly, a recent study has found that glioblastoma recapitulates a normal neurodevelopmental hierarchy using single-cell RNA-sequencing, which suggests a possible origin for glioblastoma hierarchy, and helps to identify cancer stem cell-specific targets (Couturier et al., 2020).

Additionally, CIZ1 was able to detect a micrometastasis within healthy cortex. In this case, CIZ1 staining was able to pick up a very small number of cells amongst a large area of healthy tissue (Figure 3.9). This micrometastasis would not have been visible on a scan, which suggests that CIZ1 could improve the sensitivity of biopsies through identification of metastatic disease. The caveat here is that this tool would not be of use in advanced disease as many patients do not experience any symptoms with a small tumour. The average size of a tumour upon detection is approximately 3 cm diameter sphere, although this depends on the imaging technique and where the tumour is in the brain (Murray, 2012). Also, biopsies are invasive, and would not be conducted without evidence of a tumour. MRI is being used increasingly to detect brain metastases, and it has shown a significant increase in sensitivity over both computed tomography (CT) alone (Hochstenbag et al., 2000, Suzuki et al., 2004) and PET/CT (Kruger et al., 2011) for detection of small or asymptomatic metastases. However, the gold standard MRI technique of passive contrast enhancement relies on blood–brain barrier (BBB) breakdown, an approach that is more sensitive to later-stage metastases (Serres et al., 2012).

Together, these data display not only tumour specificity using CIZ1, but perhaps suggests a possible diagnostic role in detecting differences between tumour subtypes. The data we have is limited, with no longitudinal data to accompany the patient sample, and a small starting sample size. With more patient information, such as what subtype each patient sample belongs to, alongside additional patient samples, we may be able to form correlations between CIZ1 expression and glioblastoma tumour subtype.

Interestingly, in all 6 patients, CIZ1 staining was seen, albeit at varying levels. One of the clinical challenges with glioblastoma diagnosis is that there is not a universal biomarker for all subtypes. There is also a lot of overlap in biomarkers used not only between different subtypes of glioblastoma, but between other types of brain tumours also. This increases the time from biopsy to diagnosis. Having a biomarker that is universally positive for all glioblastoma patients would be greatly beneficial in terms of immediately distinguishing it from other brain tumour types. It remains to be seen whether CIZ1 has the characteristics to perform as a biomarker of specific subtypes or has the potential to detect a range of subtypes. In future, extra controls could be performed to test the specificity of the antibody staining such as a blocking peptide control for IHC work and siRNA controls for immunofluorescence work in cell lines.

### **3.4.2 Localisation of CIZ1**

Normally, CIZ1 is localised in the nucleus, where it binds to the nuclear matrix via its nuclear matrix anchor domain at the C-terminal, acting as a molecular link between the DNA replication machinery and the sub-nuclear structures that organise their function (Ainscough et al., 2007, Ridings-Figueroa et al., 2017). In females, CIZ1 foci are found at X chromosomes, as part of its role in X-chromosome inactivation by maintaining Xist RNA localisation. The consistent findings of CIZ1 as a nuclear protein is supported by the existence of its nuclear matrix anchor domain and its role in both DNA replication and X-Chromosome inactivation.

Throughout this work, a mixture of both nuclear and cytosolic localisation was found. Only one other time has cytosolic localisation of CIZ1 been found. When overexpressed individually, CIZ1 was mostly localised to the nucleus. However, when co-expressed with p21, this caused cytosolic distribution (Mitsui et al., 1999). p21 is a CDK2 inhibitor, which is interesting as when we used CDK2 inhibitors, CIZ1 levels decreased. In this case, it does not offer a reasonable explanation in line with our observations in later experiments.

The presence of cytoplasmic CIZ1 distribution in an otherwise nuclear protein raises the question as to whether this has any implication in terms of disease pathogenesis. Analysis of the localisation of CIZ1 in neural cells and glioblastoma cells showed that CIZ1 is localised in both the nucleus and cytoplasm in human tissue samples. The cytoplasmic CIZ1 found may be the result of translation of CIZ1 protein in the cytoplasm prior to localisation to the nucleus or may reflect aberrant localisation associated with disease. Other instances where CIZ1 localisation is not solely nuclear is when co-expressed with p21, resulting in cytosolic distribution (Mitsui et al., 1999), and when CIZ1-F protein expression patterns changed on entry to quiescence, switching from nuclear localisation in cycling cells, to nuclear exclusion with cytoplasmic signal at confluence, to nearly undetectable in quiescence (Swarts et al., 2018). In addition, splice variants may lack the nuclear localisation sequence (NLS) that prevents transport to the nucleus. This could be determined using RNA sequencing to establish whether these sequences are lost in glioblastoma. Nevertheless, the lack of staining found in the nucleus at times was unexpected and may reflect altered functions in glioblastoma.

Results of this chapter indicate that CIZ1 appears to be overexpressed in tumour patient with glioblastoma, and anti-CIZ1 stain appears to be tumour specific. Going forward, detailed stratification of patients and selection based on CIZ1 staining would be useful in determining whether CIZ1 IHC staining is representative of all subtypes. This analysis shows that CIZ1

may be a useful biomarker, as it is able to distinguish between healthy and tumour regions. However, at present there is no information regarding the classification of disease. In particular, this study does not use representative tumour sections from each of the 4 classifications of glioblastoma (classical, mesenchymal, proneural and neural). Consequently, analysis of a larger patient cohort with full details on classification and molecular biomarkers is also required to determine if CIZ1 is a bona fide biomarker in glioblastoma.

**Chapter 4: Modulation of CIZ1  
expression with CDK and DDK small  
molecule inhibitors.**

## 4.1 Introduction

Numerous cancers have shown to be dependent on overexpression of CIZ1 for tumour growth such as breast, colorectal and prostate (den Hollander et al., 2006, Higgins et al., 2012, Nishibe et al., 2013, Pauzaite et al., 2016, Yin et al., 2013, Zhang et al., 2015, Zhou et al., 2018). The precise mechanism remains to be fully understood, but there appears to be adaptations to the cell cycle that makes tumour cells dependent on high levels of CIZ1 in certain contexts. The overexpression of CIZ1 appears to be an Achilles heel in this context because CIZ1 depletion reduces cancer cell migration, proliferation and tumour growth in xenograft models (Higgins et al., 2012, Lei et al., 2016, Wu et al., 2016, Zhang et al., 2015). These observations suggest that CIZ1 may be a potential drug target for the treatment of tumours with high CIZ1 expression levels. Having established that CIZ1 is overexpressed in glioblastoma tumours, therefore may promote proliferation in glioblastoma cells, we shall determine whether glioblastoma requires CIZ1 expression for growth. CIZ1 specific siRNAs will be used to reduce its levels and determine the effects on proliferation. In addition, it has recently been shown that CIZ1 levels can be reduced through the use of small molecular kinase inhibitors (Pauzaite, 2019). This approach will be extended to glioblastoma cell lines and primary cell lines to establish if CIZ1 levels can be manipulated pharmacologically.

In murine fibroblasts, inhibition of CDK2/DDK activity promotes Ubiquitin/Proteasome System (UPS) mediated degradation of CIZ1 (Pauzaite, 2019). This observation suggests that CDK or DDK inhibitors may be repurposed to reduce CIZ1 levels through shifting the equilibrium of opposing CDK and UPS networks that regulate CIZ1 abundance (Figure 4.1). The model proposed suggests that normal CIZ1 levels are regulated via a balance of opposing CDK/DDK and UPS networks and by targeting CDK/DDK activity, this may increase the rate of proteasomal degradation of CIZ1 (Pauzaite, 2019). Hyperphosphorylation of CIZ1 as a result of increased CDK activity may cause over-accumulation, resulting in facilitating increased rate of CIZ1 dependent cancer proliferation. Alternatively, CIZ1 may over-accumulate as a result

of the loss of function of the UPS, which is responsible for normal CIZ1 degradation, in turn also contributing to tumourigenesis.

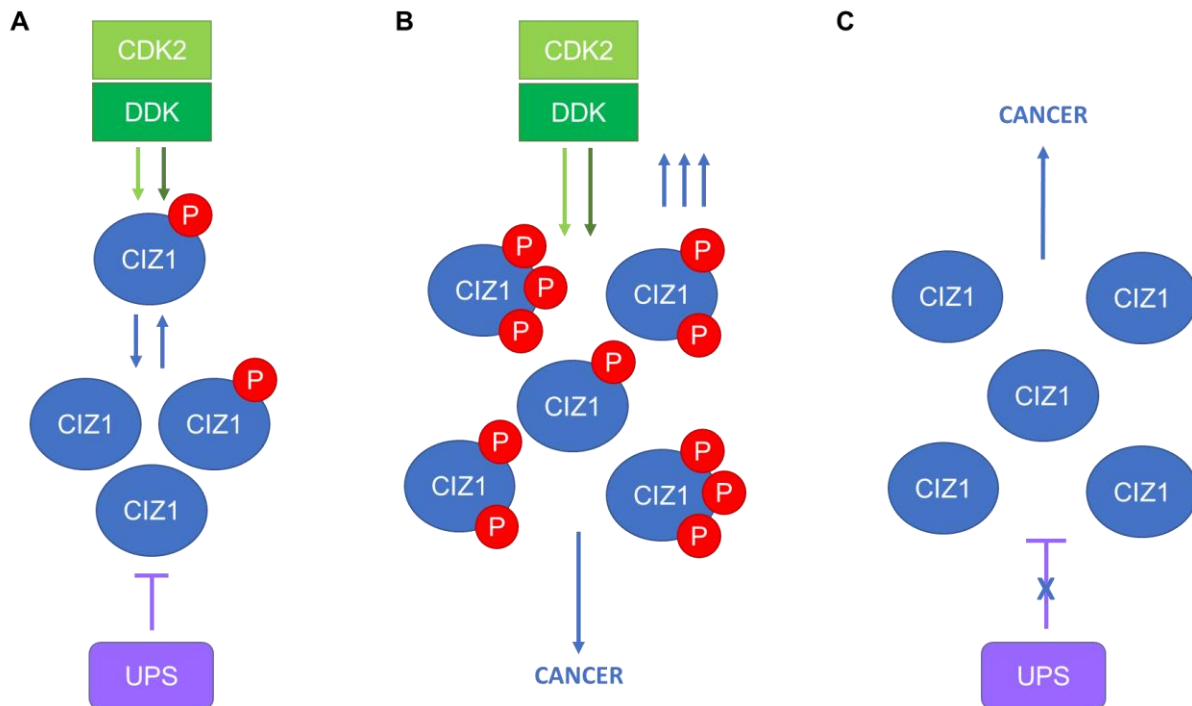


**Figure 4.1: Model of CIZ1 regulation CDK2 and DDK kinase activity and UPS mediated degradation.** **A.** Normal CIZ1 levels are regulated via a balance of opposing CDK/DDK and UPS networks. CDK2 and DDK phosphorylation of CIZ1 protects it from degradation, thus positively contributing to CIZ1 accumulation in G1 phase. CIZ1 level is downregulated by UPS mediated degradation, providing tight regulation of CIZ1 abundance in the cell cycle. **B.** Increased CDK activity may lead to CIZ1 hyperphosphorylation, which in turn leads to CIZ1 over-accumulation facilitating increased rate of CIZ1 dependent cancer proliferation. **C.** Mutations and loss-of-function in UPS responsible for normal CIZ1 degradation leads to over-accumulation of CIZ1 contributing to tumourigenesis. Figure adapted from (Pauzaitė, 2019).

Although this model predicts that CDK inhibitors may reduce CIZ1 levels, this study will also assess the use of DDK and CDK4/6 inhibitors. There is rationale for testing CDK4/6 inhibitors as numerous studies have clearly established that the cell cycle kinases CDK4 and CDK6 are activated during the pathogenesis of glioblastoma (Michaud et al., 2010, Schroder and McDonald, 2015). A phase I study found CDK4/6 inhibitor ribociclib penetrated recurrent glioblastoma tissue at concentrations predicted to be therapeutically beneficial. Although well tolerated, ribociclib monotherapy seemed ineffective for the treatment of recurrent

glioblastoma. A phase II trial also found CDK4/6 inhibitor palbociclib monotherapy was not an effective treatment for recurrent RB1 positive glioblastoma. However, the patients in this trial were heavily pre-treated patients and targeting the CDK4/6 pathway may still deserve further exploration (Taylor et al., 2018). There are more promising data showing synergistic efficacy of some CDK4/6 inhibitors in combination with other inhibitors, such as mTOR inhibitors (Olmez et al., 2017). Additionally, efficacy may depend on tumour subtype, as there is evidence that CDK4/6 inhibitors may be increased active inhibition in proneural subtypes (Li et al., 2017). Overall, CDK4/6 inhibitors still show promise for effective clinical use. This chapter will provisionally evaluate the role of CIZ1 in glioblastoma proliferation firstly through use of specific siRNAs, followed by the use cyclin dependent kinase inhibitors (CDKis) and DBF4-dependent kinase inhibitors (DDKis).

## **4.2 Transfecting Neural Cells**

### **4.2.1 BTNW914 transfection optimisation**

Using siRNA to reduce CIZ1 levels is an approach that has been used both in vitro and in vivo, successfully causing a corresponding reduction in tumour growth in mouse models (Higgins et al., 2012, Liu et al., 2015, Wu et al., 2016) and cellular proliferation in colorectal cancer (Yin et al., 2013) and prostate cancer (Pauzaite, 2019) cell lines. The efficacy of this approach in previous studies lead to the use of this approach in primary glioblastoma cell lines.

As there was no previously established protocol for BTNW914 primary cells, a transfection optimisation protocol was used to determine if nucleofection could be used. Five programs were selected in order to optimise and select the program with the best transfection efficiency (A-003, E-013, G-013, O-017 and T-020), with a non-transfected control. Cells were transfected with GFP, and transfection efficiency was determined using immunofluorescence

microscopy. Approximately 100 nuclei were counted per transfection program. Of the five programs chosen to use for nucleofection, four of the programs (A-003, E-013, G-013 and O-017) displayed very little transfection efficacy with low GFP percentage (Figure 4.2: B). However, program T-020 had a notably higher percentage of 45.5%. As this was found to be the most effective transfection program, it was selected to go forward with siRNA experiments.

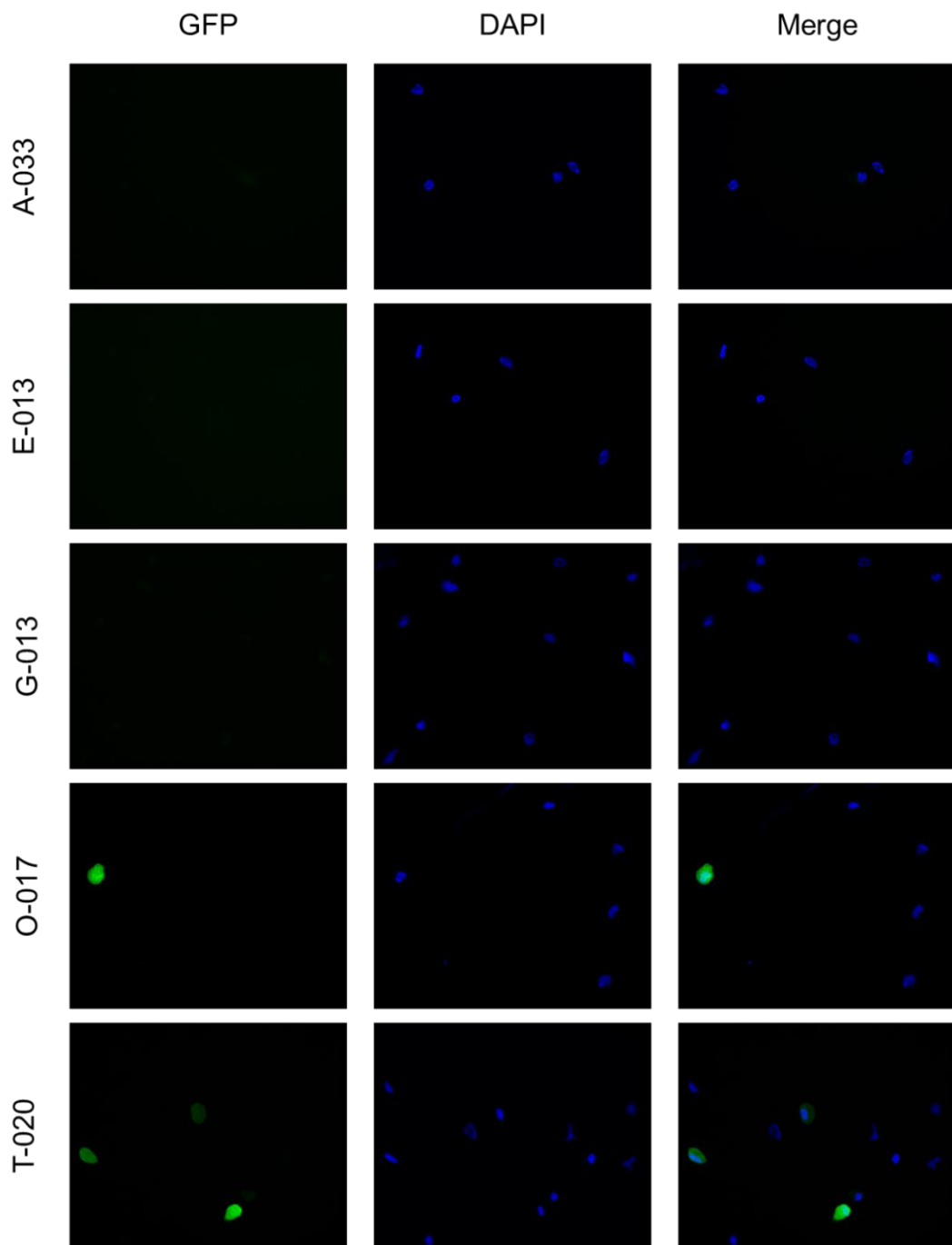


**Figure 4.2: Immunofluorescent images of GFP transfected BTNW914 cells.** BTNW914 transfection optimisation. Cells were transfected with GFP using Nucleofector programs A-033, E-013, G-013, O-017 and T-020. Images showing GFP transfected nuclei.

<b>Program</b>	<b>% of cells with GFP</b>
A-033	6%
E-013	2%
G-013	7.7%
O-017	11.4%
T-020	45.5%
No transfection	0%

**Table 4.1: Percentage of GFP transfected BTNW914 cells per program.** Table with percentages of approximately 100 nuclei which were successfully transfected with GFP using Nucleofector programs A-033, E-013, G-013, O-017 and T-020, or no transfection.

#### **4.2.2 CIZ1 depletion effects**

Having optimised a transfection protocol for BTNW914 cells, the next aim was to determine the effect of reducing CIZ1 levels in these cells (Figure 4.3). To ensure CIZ1 had been effectively reduced, Western blotting was used to determine protein levels and qPCR determine mRNA transcript levels. Western blot analysis displayed a marked reduction of CIZ1 relative to the control (Figure 4.3: A). In addition, there was also a markedly reduced CIZ1 mRNA transcript level relative to control samples (Figure 4.3: B). Together, the data show that the transfection has been successful in reducing CIZ1.

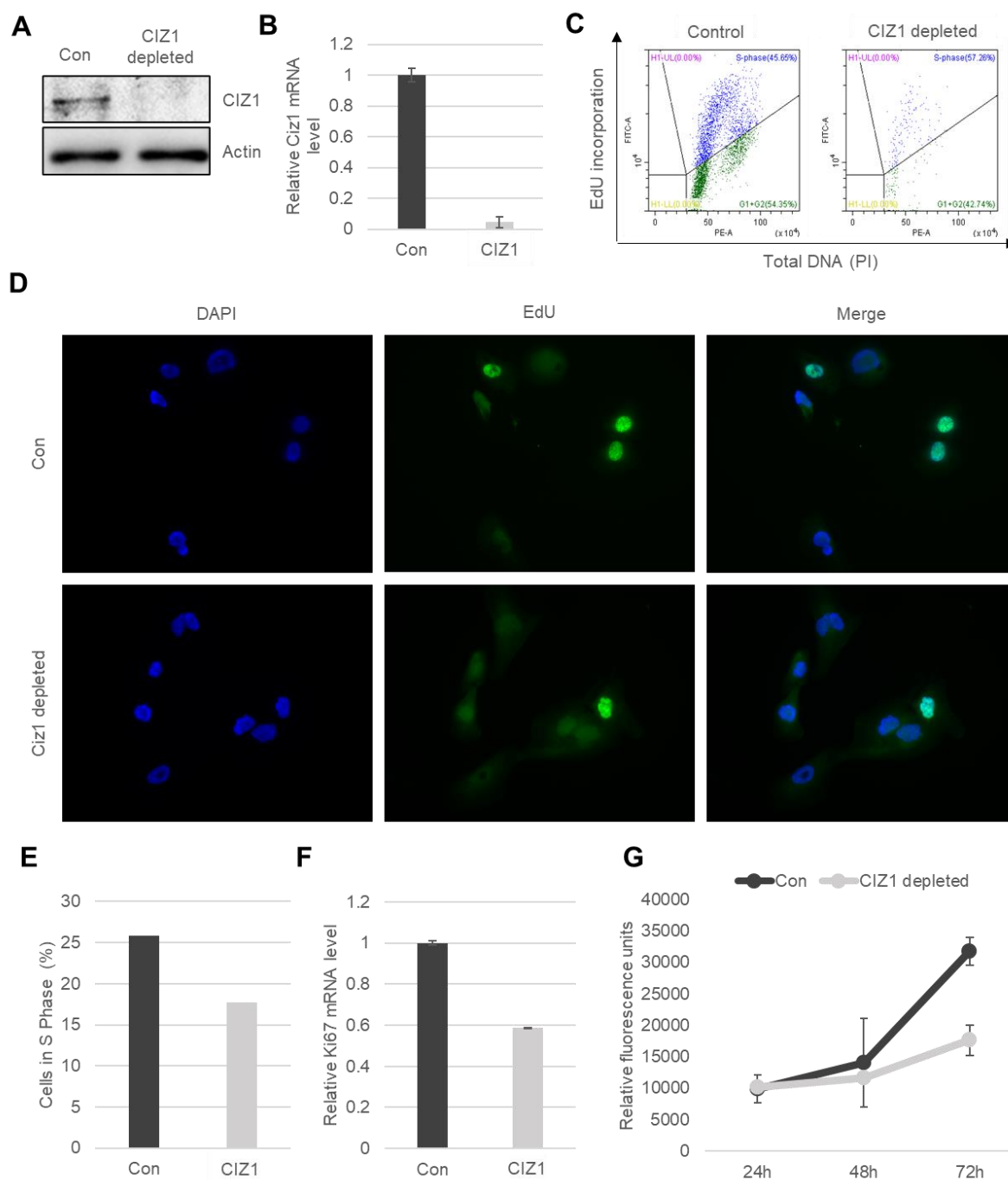


**Figure 4.3: Anti-CIZ1 siRNA transfection of BTNW914 cells.** Cells were transfected with anti-CIZ1 siRNA. **A.** Cells were harvested after 24 hours. Western blot probed for CIZ1 and Actin. **B.** CIZ1 mRNA levels were quantified by qPCR relative to GAPDH. Data shows the mean and standard deviation for 3 technical replicates where n=1. **C.** Multiparameter flow cytometry dot plot showing EdU intensity of nascent DNA (EdU-alexafuor 488) (y-axis) vs total DNA (PI) (x-axis). **D.** Representative immunofluorescence images showing reduction of S phase entry of CIZ1 depleted cells compared to control. **E.** Percentage of cells in S-phase calculated from approximately 100 nuclei using immunofluorescence. **F.** Ki67 mRNA levels were quantified by qPCR relative to GAPDH. Data shows the mean and standard deviation for 3 technical replicates where n=1. **G.** PrestoBlue proliferation assay performed after 24, 48 and 72 hours. Data shows the mean and standard deviation for 3 technical replicates where n=1.

Having established that the transfection was successful in reducing CIZ1 transcript and protein levels, the next aim was to analyse the effects of CIZ1 depletion on S phase entry in BTNW914 cells. Samples were analysed by flow cytometry and immunofluorescence. Cells were pulse labelled with EdU and fluorescently labelled using the Click-it reaction adding Alexa Fluor (488 for flow and 555 for microscopy) Azide. This allowed the visualisation of cells that were actively replicating their DNA. Using fluorescence microscopy, approximately 100 nuclei were counted per sample, counted how many were positively labelled, then calculated a percentage (Figure 4.3D, E). An 8.1% decrease in EdU incorporation was seen in CIZ1 depleted cells, from 25.8% of cells to 17.7% (Figure 4.3: E). This shows there is a decrease in S phase entry of CIZ1 depleted cells. Flow cytometry analysis of cells pulse labelled 1 hour prior to harvest with EdU and counterstained with propidium iodine (PI) was performed on samples harvested after 24 hours (figure 4.3: C). In contrast to the immunofluorescence data, flow cytometry analysis shows slight increase in S phase cells, from 45.65% cells in S phase in the control, to 57.26% in the CIZ1 depleted sample. This could simply be explained by the lack of cell numbers in the CIZ1 depleted sample, and further replicates are required to ensure reproducibility. Alternatively, this could be explained by a reduced rate of DNA synthesis. As this is a measure of the percentage of cells in S-phase and does not necessarily correlate with the rate of cell division, a proliferation assay that reports directly on cell number and quantification of the proliferation marker, Ki67, was also determined.

Reducing CIZ1 levels in different cancer types reduces *in vitro* proliferation in numerous other cancers (Pauzaite, 2019). In determining whether BTNW914 glioblastoma cells were dependent on CIZ1 for proliferation, Ki67 transcript levels were used as a proliferation marker (Figure 4.3: F). In addition, metabolic activity of cells was measured over 72 hours using a PrestoBlue assay, which was also used to determine proliferation rate (Figure 4.3: G). qPCR results show a reduction in Ki67 mRNA transcript levels relative to control levels, which would

suggest a reduction in proliferation. A PrestoBlue assay was also performed to determine the effects of the CIZ1 depletion on proliferation (Figure 4.3: G). PrestoBlue reagent is reduced by metabolically active cells, that provides a fluorimetric change indicative of the number of live cells present in a sample. The PrestoBlue reagent was added to each well 1 hour prior to inserting into the plate reader. Starting with 5000 cells per well, relative fluorescence levels were measured over 72 hours, allowing us to observe the changes in proliferation between control and CIZ1 depleted samples. Both the control and depleted sample have similar cell numbers at 24h but shows a greater increase in proliferation of control cells over CIZ1 depleted ones over 72 hours. The data suggest that reduction of CIZ1 appears to slow proliferation in this context and further replicates are required here to ensure reproducibility of this observation.

## **4.3 Reduction of CIZ1 levels by CDK/DDK inhibition**

### **4.3.1 Proof of principle using SW620 cells**

The data presented (Figure 4.3) suggests that reduction of CIZ1 levels may reduce cellular proliferation in vitro. As the use of genetic tools to reduce CIZ1 expression is not viable for the treatment of glioblastoma, the use of conventional pharmaceutical intervention may provide a more suitable approach. The principle for reducing CIZ1 levels by CDKis and DDKis has been demonstrated in fibroblasts (Pauzaite, 2019). The aim of using SW620 cells is to validate this method, and to test if the outcome can be replicated in multiple cell/cancer types.

Cells were treated with Palbociclib Isethionate (PD0332991, hereafter called PD), PHA-767491 (PHA), XL-413 (XL), Roscovitine (Ros) and CVT-313 (CVT) to analyse the effects on CIZ1 protein levels and site-specific phosphorylation of Ciz1 CDK phosphorylation site T293, and to analyse its effect on S phase entry. PD is a currently approved breast cancer treatment (Palbociclib) and is a highly selective inhibitor of CDK4 and CDK6 (Fry et al., 2004, De Luca

et al., 2018). All inhibitors used here are ATP analogue competitive inhibitors that block ATP binding to CDKs through direct competition (Law et al., 2015). Ros inhibits CDKs through direct competition at the ATP-binding site. Ros is a broad-range purine inhibitor, which inhibits CDK1, CDK2, CDK5 and CDK7, but is a poor inhibitor for CDK4 and CDK6 (Cicenas et al., 2015). CVT is a potent and specific CDK2 inhibitor, although can also inhibit CDK1 at higher concentrations (Brooks et al., 1997). Both PHA and XL are DDKis that affect replication fork progression (Rainey et al., 2017, Rodriguez-Acebes et al., 2018), but by differing mechanisms. PHA inhibits initiation of DNA replication (Rodriguez-Acebes et al., 2018), whereas XL affects fork progression without affecting initiation of DNA replication (Alver et al., 2017). Each kinase has off target effects (Table 4.1).

Drug	Target	IC50 in cell free assays	Off target effects	IC50 of off target
Palbociclib (PD0332991) Isethionate	CDK4 CDK6	11 nM 16 nM	None	N/A
PHA-767491 dihydrochloride	Cdc7	10 nM	CDK9 CDK2	34 nM 240 nM
XL-413 hydrochloride	Cdc7	3.4 nM	None	N/A
Roscovitine	CDK2	0.7 $\mu$ M	Cdc2 CDK5	0.65 $\mu$ M 0.16 $\mu$ M
CVT-313	CDK2	0.5 $\mu$ M	None	N/A

**Table 4.2: Summary of small molecule inhibitors used.** The table indicates the drugs used in the experiments, their main targets and activity expressed as IC50.

Initially as a proof of principle, colorectal carcinoma cells SW620 were treated with CDK4/6 (PD), DDKis (PHA and XL), and CDK2 inhibitors (Ros and CVT) to analyse the effects on CIZ1 protein levels and site-specific phosphorylation of CIZ1 CDK site pT293, and to analyse the effects on S phase entry. SW620 cells were treated with CDKis and DDKis, then harvested at 7 hours and 24 hours and probed for CIZ1, pCIZ1, MCM2 and pS53 (Figure 4.6: A). These

timepoints were selected to represent an acute and long timepoint, with the acute 7 hour timepoint capturing cells in different phases of the cell cycle, and the 24 hour timepoint allowing observation after a full cell cycle. Western blot analysis for SW620 cells revealed a reduction in CIZ1 T293 phosphorylation at both 7 hours and 24 hours for DDKi PHA, and CDKis Ros and CVT that resulted in lowered CIZ1 protein levels after 24 hours treatment. This may suggest a possible time lag for the effects of reduction in phosphorylation and decrease in CIZ1 protein. Importantly, MCM2 levels remained constant that serves as a load control and as a DDK specific phospho-site (pS53) that was only reduced by DDK inhibitors PHA and XL.

To analyse the effects of CDKi and DDKi on S phase entry in SW620 cells, flow cytometry analysis of cells pulse labelled with EdU and counterstained with propidium iodine (PI) was performed on samples harvested after 7 hours and 24 hours (Figure 4.6: B). This showed a lower proportion of cells in S phase with Ros and CVT treatment after 7 hours. This effect was enhanced after 24 hours treatment, resulting in greatly reduced proportion of cells in S phase with PHA, Ros and CVT treatment (Figure 4.4). Flow cytometry results show a substantial reduction in cell cycle progression with PHA, Ros and CVT. There is also a reduction in G2 cells with XL treatment (Figure 4.4: B). PD also shows a small reduction compared to control. Overall, the data show that the DDK inhibitor PHA767491 as well as the CDK2 inhibitors Ros and CVT efficiently reduce CIZ1 protein levels and arrest cells in G1 and G2 phases with a reduction in S phase cells. Importantly, there is a strong correlation between the efficacy of CIZ1 reduction and the proliferative potential of the cells.

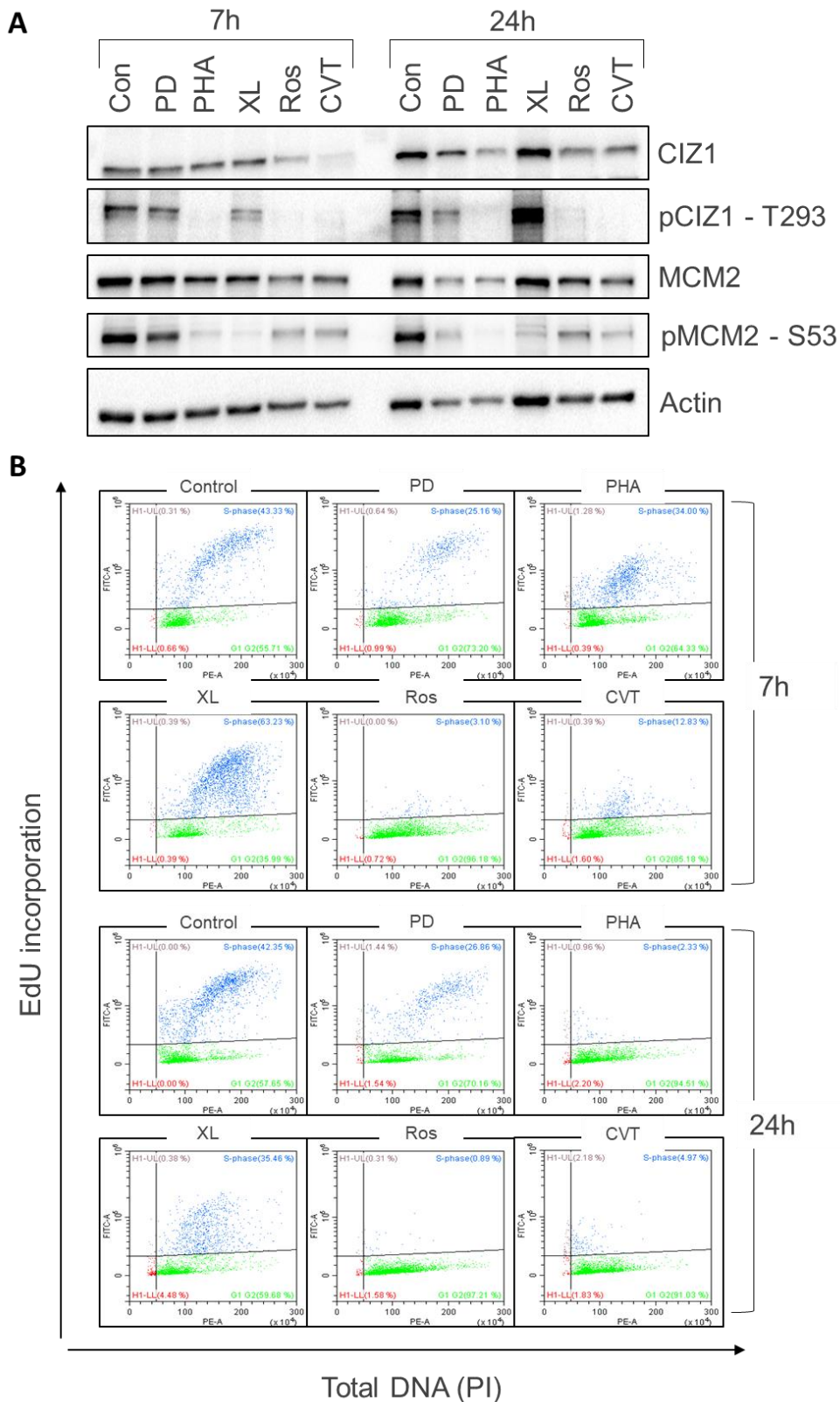


**Figure 4.4: Treating SW620 cells with CDKis and DDKis.** Cells were treated with PD, PHA, XL, Ros and CVT. **A.** Cells were treated with drugs for 7 and 24 hours. Western blots were probed with CIZ1, pCIZ1-T293, MCM2, pMCM2-S53 and Actin. **B.** Multiparameter flow cytometry dot plot showing EdU intensity (y-axis) vs total DNA (x-axis) assessing the effect of each drug on cell cycle profile and entry to S-phase. Data shows n=1.

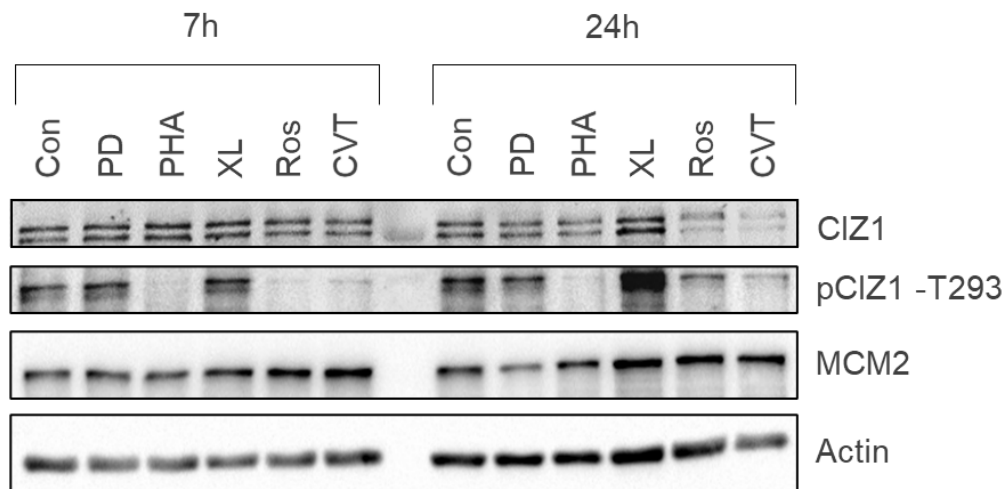
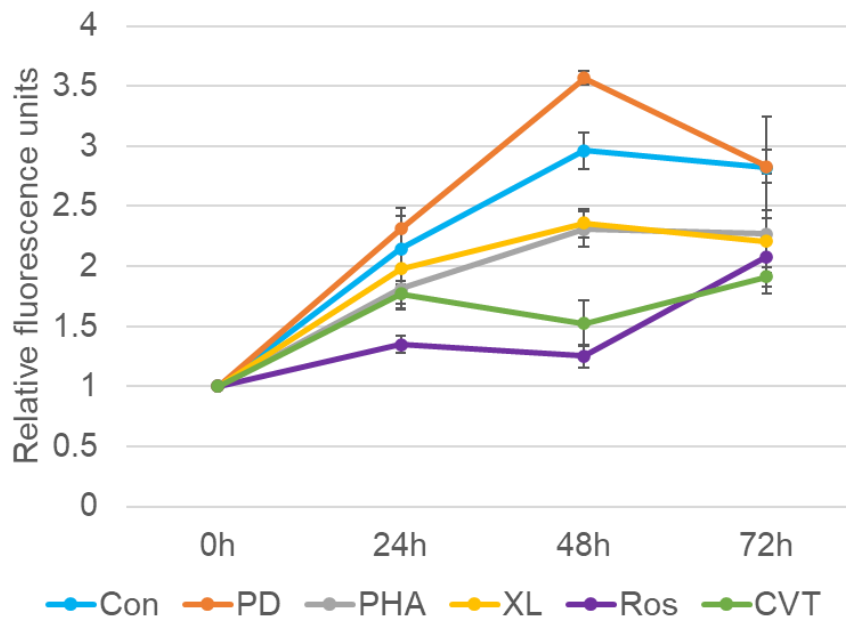
### 4.3.2 Neural cells

Having established a proof of principle in being able to show that CDK and DDK inhibition reduces CIZ1 levels in other cancer types, this approach was evaluated in BTNW914 primary glioblastoma, U87MG and transformed glia SVGp12 cells. CIZ1 protein levels were evaluated after inhibitor treatment, as was the rate of proliferation. Proliferation was measured in relation to CIZ1 expression as it has an important role in the control and promotion of DNA replication, and interacts with cyclins, coordinating their function (Copeland et al., 2010). CIZ1 is also a CDK sensor that promotes initiation of DNA replication and prevention of re-replication (Copeland et al., 2015). Measuring rate of proliferation shows that CDKis and DDKis may be reducing CIZ1, which in turn should reduce proliferation. However, it is important to keep in mind that inhibiting CDKs would likely in themselves reduce proliferation as they are key components of the cell cycle.

Cells were treated with CDK4/6 (PD), DDKis (PHA and XL), and CDK2 inhibitors (Ros and CVT). Cells were harvested at 7 hours or 24 hours and probed for CIZ1, pCIZ1 and MCM2. Western blots from BTNW914 cells (figure 4.5: A) revealed CIZ1 levels are reduced at 24 hours when treated with PHA and Ros. Interestingly, a reduction in CIZ1 with PD at 24 hours is now seen. It is worth noting that a fresh batch of PD was used, which appeared to be more potent compared to the original batch. This may explain the sudden decrease seen in CIZ1 levels that have not been seen up to this point. In contrast with earlier results, CVT did not reduce CIZ1 or levels of pT293 which may be the result of a failure of response in this cell line. To determine the effects of the drugs on proliferation, a PrestoBlue assay was performed. This showed that the control, PD and XL samples showed an increase in proliferation, whereas there was a reduction in proliferation with PHA, Ros and CVT treatment (Figure 4.5B). The results show that there is a correlation between CIZ1 levels that correlates with phosphorylation of CIZ1. However, when measuring proliferation, there is a correlation between CDK2 inhibition and proliferation as Ros, CVT and PHA are all CDK2 inhibitors with



pCIZ1, MCM2 and pS53. In contrast to the BTNW914 cells, the addition CDK or DDK inhibitors appears to have a minimal impact on CIZ1 levels at both 7 hours and 24 hours. A slight decrease is seen with CVT, and a smaller decrease with Ros. This may be because this cell line is less sensitive to these drugs due to an unknown mechanism, or perhaps 24 hours is not be enough time for CIZ1 degradation. Reduction in T293 phosphorylation is seen with PHA, Ros and CVT treatment, similar to what we have seen in all BTNW914 and SW620 cells. Strangely, at 24 hours, there also seems to be an increase in both CIZ1 and CIZ1 phosphorylation with XL, although this may be due in part to a slightly uneven sample load compared to control. Overall, there is a less reduction in CIZ1 expression in U87MG cell lines between the control and DDK kinase inhibitor treatments, but there is a reduction when using CDK2 inhibitors Ros and CVT. The PrestoBlue proliferation assay shows a moderate reduction in proliferation with PHA, XL, Ros and CVT relative to control (Figure 4.6B). The inhibition of CDK4/6 does not appear to affect proliferation with proliferation rates similar to control at 48 and 72 hours. However, in contrast to the Western blot, proliferation is reduced with XL as well.

**A****B**

**Figure 4.6: Treating U87MG cells with CDKis and DDKis.** Cells were treated with PD, PHA, XL, Ros and CVT. **A.** Cells were treated with drugs for 7 and 24 hours. Western blots were probed with CIZ1, pCIZ1-T293, MCM2 and Actin. **B.** PrestoBlue assay was performed after 0, 24, 48 and 72 hours. Data shows the mean and standard deviation for 3 technical replicates where n=1.

After comparing the effects of the drugs on glioblastoma cell lines, cell line SVGp12 cells were used as a 'normal' control. Western blot results show PHA, Ros and CVT treatment reduced CIZ1 protein levels, and there is also a reduction for CIZ1 levels after XL treatment that contrasts with glioblastoma primary cells and cell lines. Consistent with reduction in CIZ1 levels correlating with reduced proliferation, PHA, Ros and CVT all reduced proliferation, and

XL also showed a moderate reduction in proliferation, mirroring the loss of CIZ1 from the Western blot. Proliferation with PD jumps up above the control rate of proliferation, in a similar pattern to what we see with U87MG cells.

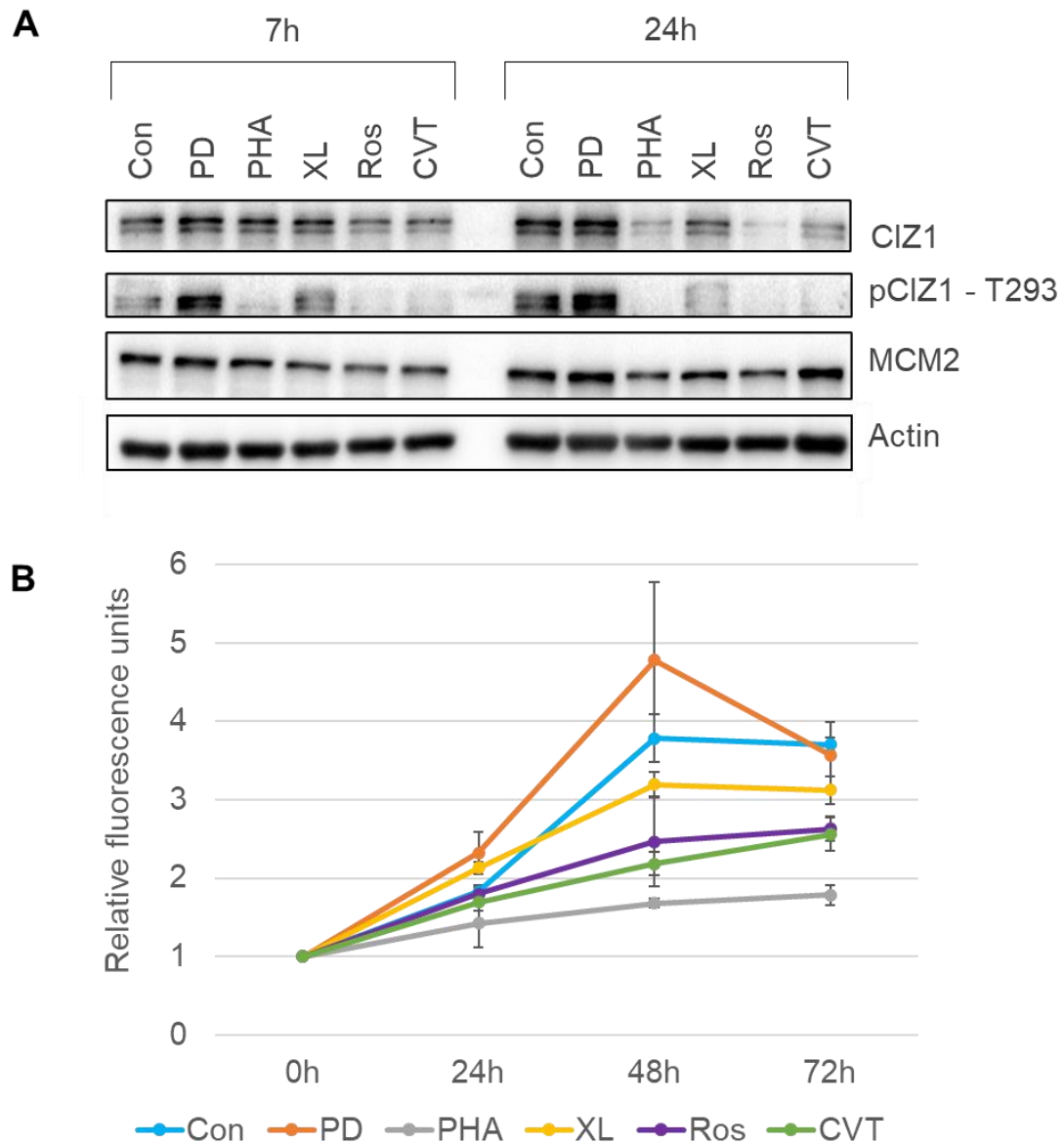


**Figure 4.7: Treating SVGP12 cells with CDKis and DDKis.** Cells were treated with PD, PHA, XL, Ros and CVT. **A.** Cells were treated with drugs for 7 and 24 hours. Western blots were probed with CIZ1, pCIZ1-T293, MCM2 and Actin. **B.** PrestoBlue assay was performed after 0, 24, 48 and 72 hours. Data shows the mean and standard deviation for 3 technical replicates where n=1.

## 4.4 Chapter Discussion

### 4.4.1 Knockdown of CIZ1 reduces proliferation and cell cycle progression

CIZ1 contributes to tumorigenesis in a number of tumours including breast (den Hollander et al., 2006), colorectal (Wang et al., 2014, Yin et al., 2013), hepatocellular carcinoma (Wu et al., 2016), gall bladder (Zhang et al., 2015), prostate (Liu et al., 2015), small cell lung and non-small cell lung carcinoma (Higgins et al., 2012). In each case, CIZ1 has been implicated directly in tumour growth due to overexpression or alternative splicing (Higgins et al., 2012, Swarts et al., 2018).

Using siRNA to reduce CIZ1 levels is an approach that has been used both *in vitro* and *in vivo*, successfully causing a corresponding reduction in tumour growth in mouse models (Higgins et al., 2012, Liu et al., 2015, Wu et al., 2016) and cellular proliferation in colorectal cancer (Yin et al., 2013) and prostate cancer (Pauzaite, 2019) cell lines. The efficacy of this approach in previous studies lead to the justification and reasoning for using this approach on glioblastoma cells. Consistent with earlier reports, depletion of CIZ1 reduced proliferation in BTNW914 primary glioblastoma cells as reported by reduction in KI67 and proliferation assays. However, this information comes from only one data set, therefore more repeats would be needed to validate this. Additionally, in future work, at least 2 independent CIZ1 siRNAs should be used in order to confirm phenotypes observed are not off-target effects a particular siRNA. Nonetheless, as there are currently no effective treatments for glioblastoma, demonstrating that a reduction in CIZ1 is able to reduce proliferation is a promising start, especially as these results follow the same patterns as previous works. These results suggest that approaches that reduce CIZ1 levels may be beneficial for the treatment of glioblastoma.

#### 4.4.2 CDK and DDK inhibitors reduce CIZ1 and proliferation

CDKis and DDKis have been previously shown to reduce CIZ1 levels and proliferation. (Pauzaite, 2019). The use of CDK inhibitors is based on the proposed model, which predicts that CIZ1 levels are controlled by CDKs and UPS (Figure 4.1) (Pauzaite, 2019). This model predicts that CDK activity is required for accumulation of CIZ1 and prevents UPS mediated degradation. Therefore, it predicts that inhibition of CDK activity may reduce CIZ1 levels.

In this work, we were able to establish that there is a correlation between reduction of CIZ1 by CDK and DDK inhibitors and proliferation. In particular, PHA, Ros and CVT resulted in decrease CIZ1, with a decrease in proliferation seen in all three cell types used, including the normal SVGp12 cell line. In contrast, the DDK inhibitor XL413, produced inconsistent results and occasionally saw increased CIZ1 levels but also saw a decrease in proliferation with U87MG. This decrease is not seen in BTNW914 or SVGp12. This may be related to the bioavailability of the inhibitor as earlier studies have shown that XL413 is effective in only a limited number of cancer cell lines that is associated with its solubility (Sasi et al., 2014). Again, it is worth mentioning that inhibiting CDKs and DDKs would likely in themselves reduce proliferation as key components of the cell cycle, therefore need to be aware that any reduction in proliferation may be the direct result of these inhibitors. Future work looking at the UPS part of the proposed CIZ1 regulation model (Figure 4.1) may help determine to what extent proliferation is affected by CIZ1 levels.

There are currently no approved CDK2 inhibitors, preventing the use of CDK2 inhibition in glioblastoma in clinical studies. However, PD is approved for clinical use. Its current use is in the treatment of in breast cancer in post-menopausal women that is oestrogen receptor positive and HER2 negative (De Luca et al., 2018). There was one instance where the effects on proliferation and cell cycle progression seen with PD were similar to that seen with PHA, Ros and CVT (Figure 4.5). In this instance, a new batch of PD was made up and used. This new batch was made up to a concentration that would be considered clinically relevant.

Multiple repeats and experiments would be necessary to test and validate this, but this provides evidence for the use of CDK inhibitors as potential strategy for the treatment of glioblastoma.

The experiments conducted throughout provides evidence that supports the model that predicts that CIZ1 is regulated by opposing CDK and UPS activity (Figure 4.1). This model suggests avenues to specifically reduce CIZ1 levels through modulation of UPS activity. This work extends the observations of its potential in colorectal, prostate and breast cancers (Pauzaite, 2019). However, it would make a more complete picture of the model to be able to conduct experiments which showed that blocking the UPS system would result in an increase in CIZ1 due to the inability to degrade it. The identification of the E3 ligases are involved would be of great benefit as there is potential that this knowledge could be used to identify patients that may benefit from this strategy. This information would allow us to have a better understanding of how CDKis and DDKis work in reducing CIZ1 levels.

Additional work is required to expand the analysis of the use of CDK inhibitors. Although only one repeat was successfully carried out, it showed great promise in reducing proliferation in tumour cells. Repeating this will hopefully provide the evidence needed. Use of CDK inhibitors as a potential cancer treatment is expanding. Palbociclib is a CDK4/6 inhibitor which is currently approved for use in certain breast cancers. Dinaciclib is another potent CDK inhibitor which was granted orphan drug FDA status in 2011, and is currently in clinical trials for numerous cancer types, including stage III clinical trials for chronic lymphoblastic leukaemia (Ghia et al., 2017). Dinaciclib also shows promise for myeloma treatment (Kumar et al., 2015). Additionally, expanding upon the proliferation assay to include more assays such as migration, invasion and cell death would give greater insight into how effective using CDK and DDK inhibitors as a potential treatment may be. *In vivo* work to support evidence found so far may

be considered if the trend continues. Taken together, this work shows that CIZ1 is a potential target in glioblastoma, and there is future potential for using CDKis as treatment.

## **Chapter 5: General Discussion**

## **5.1 Implications of the work**

This work has evaluated the potential for CIZ1 as a diagnostic biomarker for glioblastoma. A strong and clear distinction was seen in CIZ1 staining between tumour and non-tumour sections in 3 of the 6 FFPE sections. In the other 3 sections, CIZ1 staining was still apparent, but less clear and striking. Nonetheless, CIZ1 was able to identify tumour areas specifically in all 6 patients. CIZ1 also identified and enhanced visualisation of micrometastases and clonal variation within a tumour area. Taken together, this work gives a strong case for potential future use of CIZ1 as a diagnostic biomarker. This could be beneficial as there is a lack of a unifying biomarker specific to glioblastoma. As a highly heterogenous cancer, having this biomarker could help accelerate the diagnostic process.

## **5.2 Limitations and future work**

This work has made headway into the use of CIZ1 as a biomarker. The major limitation to this section of the work is that only 6 FFPE tumours were used for IHC analysis. In future works, using a significantly increased number of patient samples to perform IHC would allow us to determine the efficacy and sensitivity of the assay, and have a much better understanding of the potential role CIZ1 has in glioblastoma. From the samples used, we were able to conclude that there does appear to be a relationship between CIZ1 expression and tumour occurrence.

There is a strong case for CIZ1 as a biomarker, but this is currently limited to diagnosis. It may be feasible to relate CIZ1 staining to patient outcome. The work presented here demonstrates that CIZ1 is expressed at high levels and aberrantly localised. However, the prognostic potential of CIZ1 remains to be addressed. There is a need to use longitudinal data to determine the consequences of high CIZ1 levels. Here, 6 patient samples were used. In future experiments, more samples would give us more information and more data to draw stronger conclusions from. Due to lack of longitudinal data, age and sex to accompany each patient

sample used, we were unable to draw any conclusions as to whether CIZ1 expression has an impact on prognosis. Going forward, collecting this data would be useful. Additionally, extra controls could be performed to test the specificity of the antibody staining such as a blocking peptide control for IHC work and siRNA controls for immunofluorescence work in cell lines.

It would also be of interest to see whether there is a link between the tumour subtype (classical, mesenchymal, neural, proneural) and CIZ1 levels, and whether CIZ1 labels them differently. Having access to data such as which biomarkers were used for diagnosis and tested positively and negatively would be useful in determining which subtype each patient came under, and whether there is a correlation between CIZ1 and a particular subtype. As some patients respond better to certain treatments according to which glioblastoma subtype they have, CIZ1 may also be used as both a diagnostic and prognostic biomarker and may help direct personalised treatment.

The mislocalisation of CIZ1 is yet to be understood. There are a number of possible explanations for the aberrant expression of CIZ1 seen in glioblastoma. One possible reason is glioblastoma cells suffer a loss of nuclear localisation signal (NLS) due to splicing. It is unknown how changes in localisation affect its function as most described functions are nuclear. Loss of nuclear function is a possibility in this scenario. Additionally, we have found that not only glioblastoma cells show mislocalisation. Normal glial cells also have cytosolic distribution in addition to nuclear according to our fractionation and immunofluorescence data. Neurons also display cytosolic localisation as seen in our IHC data. Endothelial cells also show CIZ1 stain, but from our data, it appeared only to show stain when within a tumour area. In future work this would be worth exploring as this might have an implication in disease pathogenesis.

The work on the modulation of CIZ1 shows efficacy of CDKi/DDKi leading to CIZ1 reduction, alongside the proliferation assays has provided evidence for use of CDKis and DDKis in reducing proliferation of glioblastoma tumour cells. The basis for starting this work relied on the siRNA work in reducing CIZ1 and previous work where CDKis/DDKis were used effectively (Pauzaite, 2019). The siRNA work is only comprised of a single repeat, which requires further experimental validation. Additionally, expanding upon the proliferation assay to include more assays such as migration, invasion and cell death would give greater insight into how effective using CDK and DDK inhibitors as a potential treatment may be. *In vivo* work to support evidence found so far may be considered if the trend continues. The CIZ1 regulatory model (Figure 4.1) whereby CIZ1 is regulated by the opposing CDK/UPS system, suggests that use of CDK inhibitors as a potential glioblastoma treatment and necessitates additional work to fully understand how CIZ1 is regulated. The work concludes that CIZ1 may be a potential drug target in glioblastoma and additional work is required to validate its efficacy *in vitro* and *in vivo*.

### **5.3 Concluding remarks**

To conclude, this work has found that CIZ1 is specific to glioblastoma tumour cells, making it a potentially viable biomarker. More samples and accompanying patient data will reveal its potential as an effective diagnostic and prognostic biomarker.

We have found an unusual localisation pattern in these cells. Whereas CIZ1 is normally located in the nucleus, this work has found using multiple ways that CIZ1 is found in both the nucleus and cytoplasm. As of yet, the mechanism of CIZ1 mislocalisation remains to be determined. However, the mislocalisation provides aids in the visualisation of CIZ1 stained tumour cells and may enhance the ability of CIZ1 to be used as a biomarker in glioblastoma.

We have confirmed that reduction of CIZ1 correlates with a reduction in proliferation. Additionally, the use of some CDKis and DDKis that have been used to reduce CIZ1 levels

previously in different cell types, also are able to do so in glioblastoma cells, in turn also resulting in reduced proliferation. These results suggest that modulation of CIZ1 levels is feasible pharmacologically and this represents a potential strategy to reduce CIZ1 levels in tumours. This approach requires new molecules that can specifically inhibit CDK2 activity that are able to show efficacy in clinical trials. At this stage, the results show promise and require extension of this work. This work demonstrates that CIZ1 may contribute to glioblastoma growth and that the use of CDKis and DDKis are able to reduce CIZ1 levels and proliferation. Consequently, there is the potential for the repurposing of similar kinase inhibitors for future therapeutic use in glioblastoma.

# References

- AINSCOUGH, J. F., RAHMAN, F. A., SERCOMBE, H., SEDO, A., GERLACH, B. & COVERLEY, D. 2007. C-terminal domains deliver the DNA replication factor Ciz1 to the nuclear matrix. *J Cell Sci*, 120, 115-24.
- ALEXANDER, B. M. & CLOUGHESY, T. F. 2017. Adult Glioblastoma. *J Clin Oncol*, 35, 2402-2409.
- ALVER, R. C., CHADHA, G. S., GILLESPIE, P. J. & BLOW, J. J. 2017. Reversal of DDK-Mediated MCM Phosphorylation by Rif1-PP1 Regulates Replication Initiation and Replisome Stability Independently of ATR/Chk1. *Cell Rep*, 18, 2508-2520.
- AN, Z., AKSOY, O., ZHENG, T., FAN, Q. W. & WEISS, W. A. 2018. Epidermal growth factor receptor and EGFRvIII in glioblastoma: signaling pathways and targeted therapies. *Oncogene*, 37, 1561-1575.
- AVNINDER, S., SHARMA, M. C., DEB, P., MEHTA, V. S., KARAK, A. K., MAHAPATRA, A. K. & SARKAR, C. 2006. Gemistocytic astrocytomas: histomorphology, proliferative potential and genetic alterations--a study of 32 cases. *J Neurooncol*, 78, 123-7.
- BI, W. L. & BEROUKHIM, R. 2014. Beating the odds: extreme long-term survival with glioblastoma. *Neuro Oncol*, 16, 1159-60.
- BOSE, A. & DALAL, S. N. 2019. Centrosome Amplification and Tumorigenesis: Cause or Effect? *Results Probl Cell Differ*, 67, 413-440.
- BROOKS, E. E., GRAY, N. S., JOLY, A., KERWAR, S. S., LUM, R., MACKMAN, R. L., NORMAN, T. C., ROSETE, J., ROWE, M., SCHOW, S. R., SCHULTZ, P. G., WANG, X., WICK, M. M. & SHIFFMAN, D. 1997. CVT-313, a specific and potent inhibitor of CDK2 that prevents neointimal proliferation. *J Biol Chem*, 272, 29207-11.
- BURRI, S. H., GONDI, V., BROWN, P. D. & MEHTA, M. P. 2018. The Evolving Role of Tumor Treating Fields in Managing Glioblastoma: Guide for Oncologists. *Am J Clin Oncol*, 41, 191-196.
- CANCER GENOME ATLAS RESEARCH, N. 2008. Comprehensive genomic characterization defines human glioblastoma genes and core pathways. *Nature*, 455, 1061-8.
- CHEN, S. & BELL, S. P. 2011. CDK prevents Mcm2-7 helicase loading by inhibiting Cdt1 interaction with Orc6. *Genes Dev*, 25, 363-72.
- CICENAS, J., KALYAN, K., SOROKINAS, A., STANKUNAS, E., LEVY, J., MESKINYTE, I., STANKEVICIUS, V., KAUPINIS, A. & VALIUS, M. 2015. Roscovitine in cancer and other diseases. *Ann Transl Med*, 3, 135.
- CLOUGHESY, T. F., CAVENEY, W. K. & MISCHEL, P. S. 2014. Glioblastoma: from molecular pathology to targeted treatment. *Annu Rev Pathol*, 9, 1-25.
- COPELAND, N. A., SERCOMBE, H. E., AINSCOUGH, J. F. & COVERLEY, D. 2010. Ciz1 cooperates with cyclin-A-CDK2 to activate mammalian DNA replication in vitro. *J Cell Sci*, 123, 1108-15.
- COPELAND, N. A., SERCOMBE, H. E., WILSON, R. H. & COVERLEY, D. 2015. Cyclin-A-CDK2-mediated phosphorylation of CIZ1 blocks replisome formation and initiation of mammalian DNA replication. *J Cell Sci*, 128, 1518-27.
- COUTURIER, C. P., AYYADHURY, S., LE, P. U., NADAF, J., MONLONG, J., RIVA, G., ALLACHE, R., BAIG, S., YAN, X., BOURGEY, M., LEE, C., WANG, Y. C. D., WEE YONG, V., GUIOT, M. C., NAJAFABADI, H., MISIC, B., ANTEL, J., BOURQUE, G., RAGOISSIS, J. & PETRECCA, K. 2020. Single-cell RNA-seq reveals that glioblastoma recapitulates a normal neurodevelopmental hierarchy. *Nat Commun*, 11, 3406.
- COVERLEY, D., HIGGINS, G., WEST, D., JACKSON, O. T., DOWLE, A., HASLAM, A., AINSCOUGH, E., CHALKLEY, R. & WHITE, J. 2017. A quantitative immunoassay for lung cancer biomarker CIZ1b in patient plasma. *Clin Biochem*, 50, 336-343.

- COVERLEY, D., MARR, J. & AINSCOUGH, J. 2005. Ciz1 promotes mammalian DNA replication. *J Cell Sci*, 118, 101-12.
- DE LUCA, A., MAIELLO, M. R., D'ALESSIO, A., FREZZETTI, D., GALLO, M., CAROTENUTO, M. & NORMANNO, N. 2018. Pharmacokinetic drug evaluation of palbociclib for the treatment of breast cancer. *Expert Opin Drug Metab Toxicol*, 14, 891-900.
- DEN HOLLANDER, P., RAYALA, S. K., COVERLEY, D. & KUMAR, R. 2006. Ciz1, a Novel DNA-binding coactivator of the estrogen receptor alpha, confers hypersensitivity to estrogen action. *Cancer Res*, 66, 11021-9.
- DIRIL, M. K., RATNACARAM, C. K., PADMAKUMAR, V. C., DU, T., WASSER, M., COPPOLA, V., TESSAROLLO, L. & KALDIS, P. 2012. Cyclin-dependent kinase 1 (Cdk1) is essential for cell division and suppression of DNA re-replication but not for liver regeneration. *Proc Natl Acad Sci U S A*, 109, 3826-31.
- DOBES, M., KHURANA, V. G., SHADBOLT, B., JAIN, S., SMITH, S. F., SMEE, R., DEXTER, M. & COOK, R. 2011. Increasing incidence of glioblastoma multiforme and meningioma, and decreasing incidence of Schwannoma (2000-2008): Findings of a multicenter Australian study. *Surg Neurol Int*, 2, 176.
- DOMINGUES, P., GONZALEZ-TABLAS, M., OTERO, A., PASCUAL, D., MIRANDA, D., RUIZ, L., SOUSA, P., CIUDAD, J., GONCALVES, J. M., LOPES, M. C., ORFAO, A. & TABERNEIRO, M. D. 2016. Tumor infiltrating immune cells in gliomas and meningiomas. *Brain Behav Immun*, 53, 1-15.
- DOUGLAS, M. E. & DIFFLEY, J. F. 2016. Recruitment of Mcm10 to Sites of Replication Initiation Requires Direct Binding to the Minichromosome Maintenance (MCM) Complex. *J Biol Chem*, 291, 5879-88.
- DRURY, L. S., PERKINS, G. & DIFFLEY, J. F. 2000. The cyclin-dependent kinase Cdc28p regulates distinct modes of Cdc6p proteolysis during the budding yeast cell cycle. *Curr Biol*, 10, 231-40.
- DUHRSEN, L., SAUVIGNY, T., RICKLEFS, F. L., MENDE, K. C., SCHAPER, M., MATSCHKE, J., GOEBELL, E., WESTPHAL, M. & MARTENS, T. 2019. Seizures as presenting symptom in patients with glioblastoma. *Epilepsia*, 60, 149-154.
- EDWARDS, M. C., TUTTER, A. V., CVETIC, C., GILBERT, C. H., PROKHOROVA, T. A. & WALTER, J. C. 2002. MCM2-7 complexes bind chromatin in a distributed pattern surrounding the origin recognition complex in *Xenopus* egg extracts. *J Biol Chem*, 277, 33049-57.
- FRAGKOS, M., GANIER, O., COULOMBE, P. & MECHALI, M. 2015. DNA replication origin activation in space and time. *Nat Rev Mol Cell Biol*, 16, 360-74.
- FRIEDMANN-MORVINSKI, D. 2014. Glioblastoma heterogeneity and cancer cell plasticity. *Crit Rev Oncog*, 19, 327-36.
- FRY, D. W., HARVEY, P. J., KELLER, P. R., ELLIOTT, W. L., MEADE, M., TRACHET, E., ALBASSAM, M., ZHENG, X., LEOPOLD, W. R., PRYER, N. K. & TOOGOOD, P. L. 2004. Specific inhibition of cyclin-dependent kinase 4/6 by PD 0332991 and associated antitumor activity in human tumor xenografts. *Mol Cancer Ther*, 3, 1427-38.
- FUKASAWA, K. 2005. Centrosome amplification, chromosome instability and cancer development. *Cancer Lett*, 230, 6-19.
- GAN, H. K., KAYE, A. H. & LUWOR, R. B. 2009. The EGFRvIII variant in glioblastoma multiforme. *J Clin Neurosci*, 16, 748-54.
- GHIA, P., SCARFO, L., PEREZ, S., PATHIRAJA, K., DEROSIER, M., SMALL, K., MCCRARY SISK, C. & PATTON, N. 2017. Efficacy and safety of dinaciclib vs ofatumumab in patients with relapsed/refractory chronic lymphocytic leukemia. *Blood*, 129, 1876-1878.
- HAYES, J., THYGESEN, H., TUMILSON, C., DROOP, A., BOISSINOT, M., HUGHES, T. A., WESTHEAD, D., ALDER, J. E., SHAW, L., SHORT, S. C. & LAWLER, S. E. 2015. Prediction of clinical outcome in glioblastoma using a biologically relevant nine-microRNA signature. *Mol Oncol*, 9, 704-14.

- HEGI, M. E., DISERENS, A. C., GORLIA, T., HAMOU, M. F., DE TRIBOLET, N., WELLER, M., KROS, J. M., HAINFELLNER, J. A., MASON, W., MARIANI, L., BROMBERG, J. E., HAU, P., MIRIMANOFF, R. O., CAIRNCROSS, J. G., JANZER, R. C. & STUPP, R. 2005. MGMT gene silencing and benefit from temozolomide in glioblastoma. *N Engl J Med*, 352, 997-1003.
- HIGGINS, G., ROPER, K. M., WATSON, I. J., BLACKHALL, F. H., ROM, W. N., PASS, H. I., AINSCOUGH, J. F. & COVERLEY, D. 2012. Variant Ciz1 is a circulating biomarker for early-stage lung cancer. *Proc Natl Acad Sci U S A*, 109, E3128-35.
- HOCHEGGER, H., TAKEDA, S. & HUNT, T. 2008. Cyclin-dependent kinases and cell-cycle transitions: does one fit all? *Nat Rev Mol Cell Biol*, 9, 910-6.
- HOCHSTENBAG, M. M., TWIJNSTRA, A., WILMINK, J. T., WOUTERS, E. F. & TEN VELDE, G. P. 2000. Asymptomatic brain metastases (BM) in small cell lung cancer (SCLC): MR-imaging is useful at initial diagnosis. *J Neurooncol*, 48, 243-8.
- HOTTINGER, A. F., PACHECO, P. & STUPP, R. 2016. Tumor treating fields: a novel treatment modality and its use in brain tumors. *Neuro Oncol*, 18, 1338-49.
- IACOB, G. & DINCA, E. B. 2009. Current data and strategy in glioblastoma multiforme. *J Med Life*, 2, 386-93.
- JOHANSSON, P., JEFFERY, J., AL-EJEH, F., SCHULZ, R. B., CALLEN, D. F., KUMAR, R. & KHANNA, K. K. 2014. SCF-FBXO31 E3 ligase targets DNA replication factor Cdt1 for proteolysis in the G2 phase of cell cycle to prevent re-replication. *J Biol Chem*, 289, 18514-25.
- KIRSON, E. D., GURVICH, Z., SCHNEIDERMAN, R., DEKEL, E., ITZHAKI, A., WASSERMAN, Y., SCHATZBERGER, R. & PALT, Y. 2004. Disruption of cancer cell replication by alternating electric fields. *Cancer Res*, 64, 3288-95.
- KRUGER, S., MOTTAGHY, F. M., BUCK, A. K., MASCHKE, S., KLEY, H., FRECHEN, D., WIBMER, T., RESKE, S. N. & PAULS, S. 2011. Brain metastasis in lung cancer. Comparison of cerebral MRI and 18F-FDG-PET/CT for diagnosis in the initial staging. *Nuklearmedizin*, 50, 101-6.
- KUMAR, S. K., LAPLANT, B., CHNG, W. J., ZONDER, J., CALLANDER, N., FONSECA, R., FRUTH, B., ROY, V., ERLICHMAN, C., STEWART, A. K. & MAYO PHASE, C. 2015. Dinaciclib, a novel CDK inhibitor, demonstrates encouraging single-agent activity in patients with relapsed multiple myeloma. *Blood*, 125, 443-8.
- LAW, M. E., CORSINO, P. E., NARAYAN, S. & LAW, B. K. 2015. Cyclin-Dependent Kinase Inhibitors as Anticancer Therapeutics. *Mol Pharmacol*, 88, 846-52.
- LEE, Y., KOH, J., KIM, S. I., WON, J. K., PARK, C. K., CHOI, S. H. & PARK, S. H. 2017. The frequency and prognostic effect of TERT promoter mutation in diffuse gliomas. *Acta Neuropathol Commun*, 5, 62.
- LEI, L., WU, J., GU, D., LIU, H. & WANG, S. 2016. CIZ1 interacts with YAP and activates its transcriptional activity in hepatocellular carcinoma cells. *Tumour Biol*, 37, 11073-9.
- LI, K., LU, D., GUO, Y., WANG, C., LIU, X., LIU, Y. & LIU, D. 2018. Trends and patterns of incidence of diffuse glioma in adults in the United States, 1973-2014. *Cancer Med*, 7, 5281-5290.
- LI, M., XIAO, A., FLOYD, D., OLMEZ, I., LEE, J., GODLEWSKI, J., BRONISZ, A., BHAT, K. P. L., SULMAN, E. P., NAKANO, I. & PUROW, B. 2017. CDK4/6 inhibition is more active against the glioblastoma proneural subtype. *Oncotarget*, 8, 55319-55331.
- LINKOUS, A. G. & YAZLOVITSKAYA, E. M. 2011. Angiogenesis in glioblastoma multiforme: navigating the maze. *Anticancer Agents Med Chem*, 11, 712-8.
- LIU, T., REN, X., LI, L., YIN, L., LIANG, K., YU, H., REN, H., ZHOU, W., JING, H. & KONG, C. 2015. Ciz1 promotes tumorigenicity of prostate carcinoma cells. *Front Biosci (Landmark Ed)*, 20, 705-15.
- LOUIS, D. N., PERRY, A., REIFENBERGER, G., VON DEIMLING, A., FIGARELLA-BRANGER, D., CAVENEE, W. K., OHGAKI, H., WIESTLER, O. D., KLEIHUES, P. & ELLISON, D. W. 2016. The 2016 World Health Organization Classification of Tumors of the Central Nervous System: a summary. *Acta Neuropathol*, 131, 803-20.

- MAZZONE, P. J., SEARS, C. R., ARENBERG, D. A., GAGA, M., GOULD, M. K., MASSION, P. P., NAIR, V. S., POWELL, C. A., SILVESTRI, G. A., VACHANI, A., WIENER, R. S. & ONCOLOGY, A. T. S. A. O. T. 2017. Evaluating Molecular Biomarkers for the Early Detection of Lung Cancer: When Is a Biomarker Ready for Clinical Use? An Official American Thoracic Society Policy Statement. *Am J Respir Crit Care Med*, 196, e15-e29.
- MICHAUD, K., SOLOMON, D. A., OERMANN, E., KIM, J. S., ZHONG, W. Z., PRADOS, M. D., OZAWA, T., JAMES, C. D. & WALDMAN, T. 2010. Pharmacologic inhibition of cyclin-dependent kinases 4 and 6 arrests the growth of glioblastoma multiforme intracranial xenografts. *Cancer Res*, 70, 3228-38.
- MILETICH, R. S. 2016. Positron Emission Tomography and Single-Photon Emission Computed Tomography in Neurology. *Continuum (Minneapolis)*, 22, 1636-1654.
- MIMURA, S., SEKI, T., TANAKA, S. & DIFFLEY, J. F. 2004. Phosphorylation-dependent binding of mitotic cyclins to Cdc6 contributes to DNA replication control. *Nature*, 431, 1118-23.
- MITSUMI, K., MATSUMOTO, A., OHTSUKA, S., OHTSUBO, M. & YOSHIMURA, A. 1999. Cloning and characterization of a novel p21(Cip1/Waf1)-interacting zinc finger protein, ciz1. *Biochem Biophys Res Commun*, 264, 457-64.
- MONTANO, N., CENCI, T., MARTINI, M., D'ALESSANDRIS, Q. G., PELACCHI, F., RICCI-VITIANI, L., MAIRA, G., DE MARIA, R., LAROCCA, L. M. & PALLINI, R. 2011. Expression of EGFRvIII in glioblastoma: prognostic significance revisited. *Neoplasia*, 13, 1113-21.
- MULHOLLAND, S., PEARSON, D. M., HAMOUDI, R. A., MALLEY, D. S., SMITH, C. M., WEAVER, J. M., JONES, D. T., KOCIALKOWSKI, S., BACKLUND, L. M., COLLINS, V. P. & ICHIMURA, K. 2012. MGMT CpG island is invariably methylated in adult astrocytic and oligodendroglial tumors with IDH1 or IDH2 mutations. *Int J Cancer*, 131, 1104-13.
- MURRAY, J. D. 2012. Glioblastoma brain tumours: estimating the time from brain tumour initiation and resolution of a patient survival anomaly after similar treatment protocols. *J Biol Dyn*, 6 Suppl 2, 118-27.
- NICE. 2001. *Guidance on the use of temozolomide for the treatment of recurrent malignant glioma (brain cancer)* [Online]. Available: <https://www.nice.org.uk/guidance/ta23/resources> [Accessed 28/07/2020].
- NISHIBE, R., WATANABE, W., UEDA, T., YAMASAKI, N., KOLLER, R., WOLFF, L., HONDA, Z., OHTSUBO, M. & HONDA, H. 2013. CIZ1, a p21Cip1/Waf1-interacting protein, functions as a tumor suppressor in vivo. *FEBS Lett*, 587, 1529-35.
- OHGAKI, H. & KLEIHUES, P. 2005. Epidemiology and etiology of gliomas. *Acta Neuropathol*, 109, 93-108.
- OHGAKI, H. & KLEIHUES, P. 2013. The definition of primary and secondary glioblastoma. *Clin Cancer Res*, 19, 764-72.
- OLMEZ, I., BRENNEMAN, B., XIAO, A., SERBULEA, V., BENAMAR, M., ZHANG, Y., MANIGAT, L., ABBAS, T., LEE, J., NAKANO, I., GODLEWSKI, J., BRONISZ, A., ABOUNADER, R., LEITINGER, N. & PUROW, B. 2017. Combined CDK4/6 and mTOR Inhibition Is Synergistic against Glioblastoma via Multiple Mechanisms. *Clin Cancer Res*, 23, 6958-6968.
- OSTROM, Q. T., GITTLEMAN, H., FULOP, J., LIU, M., BLANDA, R., KROMER, C., WOLINSKY, Y., KRUCHKO, C. & BARNHOLTZ-SLOAN, J. S. 2015. CBTRUS Statistical Report: Primary Brain and Central Nervous System Tumors Diagnosed in the United States in 2008-2012. *Neuro Oncol*, 17 Suppl 4, iv1-iv62.
- PATEL, A. P., TIROSH, I., TROMBETTA, J. J., SHALEK, A. K., GILLESPIE, S. M., WAKIMOTO, H., CAHILL, D. P., NAHED, B. V., CURRY, W. T., MARTUZA, R. L., LOUIS, D. N., ROZENBLATT-ROSEN, O., SUVA, M. L., REGEV, A. & BERNSTEIN, B. E. 2014. Single-cell RNA-seq highlights intratumoral heterogeneity in primary glioblastoma. *Science*, 344, 1396-401.

- PAUZAITE, T. 2019. *Identification and analysis of the signalling networks that regulate Ciz1 levels in normal and cancer cell lines*. PhD, Lancaster University.
- PAUZAITE, T., THACKER, U., TOLLITT, J. & COPELAND, N. A. 2016. Emerging Roles for Ciz1 in Cell Cycle Regulation and as a Driver of Tumorigenesis. *Biomolecules*, 7.
- PEREZ-ARNAIZ, P., BRUCK, I. & KAPLAN, D. L. 2016. Mcm10 coordinates the timely assembly and activation of the replication fork helicase. *Nucleic Acids Res*, 44, 315-29.
- PHILIPS, A., HENSHAW, D. L., LAMBURN, G. & O'CARROLL, M. J. 2018. Brain Tumours: Rise in Glioblastoma Multiforme Incidence in England 1995-2015 Suggests an Adverse Environmental or Lifestyle Factor. *J Environ Public Health*, 2018, 7910754.
- RAHMAN, F., AINSCOUGH, J. F., COPELAND, N. & COVERLEY, D. 2007. Cancer-associated missplicing of exon 4 influences the subnuclear distribution of the DNA replication factor CIZ1. *Hum Mutat*, 28, 993-1004.
- RAHMAN, F. A., AZIZ, N. & COVERLEY, D. 2010. Differential detection of alternatively spliced variants of Ciz1 in normal and cancer cells using a custom exon-junction microarray. *BMC Cancer*, 10, 482.
- RAINEY, M. D., QUACHTHITHU, H., GABORIAU, D. & SANTOCANALE, C. 2017. DNA Replication Dynamics and Cellular Responses to ATP Competitive CDC7 Kinase Inhibitors. *ACS Chem Biol*, 12, 1893-1902.
- REINARTZ, R., WANG, S., KEBIR, S., SILVER, D. J., WIELAND, A., ZHENG, T., KUPPER, M., RAUSCHENBACH, L., FIMMERS, R., SHEPHERD, T. M., TRAGESER, D., TILL, A., SCHAFFER, N., GLAS, M., HILLMER, A. M., CICHON, S., SMITH, A. A., PIETSCH, T., LIU, Y., REYNOLDS, B. A., YACHNIS, A., PINCUS, D. W., SIMON, M., BRUSTLE, O., STEINDLER, D. A. & SCHEFFLER, B. 2017. Functional Subclone Profiling for Prediction of Treatment-Induced Intratumor Population Shifts and Discovery of Rational Drug Combinations in Human Glioblastoma. *Clin Cancer Res*, 23, 562-574.
- RICK, J., CHANDRA, A. & AGHI, M. K. 2018. Tumor treating fields: a new approach to glioblastoma therapy. *J Neurooncol*, 137, 447-453.
- RIDINGS-FIGUEROA, R., STEWART, E. R., NESTEROVA, T. B., COKER, H., PINTACUDA, G., GODWIN, J., WILSON, R., HASLAM, A., LILLEY, F., RUIGROK, R., BAGEGHNI, S. A., ALBADRANI, G., MANSFIELD, W., ROULSON, J. A., BROCKDORFF, N., AINSCOUGH, J. F. X. & COVERLEY, D. 2017. The nuclear matrix protein CIZ1 facilitates localization of Xist RNA to the inactive X-chromosome territory. *Genes Dev*, 31, 876-888.
- ROCK, K., MCARDLE, O., FORDE, P., DUNNE, M., FITZPATRICK, D., O'NEILL, B. & FAUL, C. 2012. A clinical review of treatment outcomes in glioblastoma multiforme--the validation in a non-trial population of the results of a randomised Phase III clinical trial: has a more radical approach improved survival? *Br J Radiol*, 85, e729-33.
- RODRIGUEZ-ACEBES, S., MOURON, S. & MENDEZ, J. 2018. Uncoupling fork speed and origin activity to identify the primary cause of replicative stress phenotypes. *J Biol Chem*, 293, 12855-12861.
- SAADATPOUR, L., FADAEI, E., FADAEI, S., NASSIRI MANSOUR, R., MOHAMMADI, M., MOUSAVI, S. M., GOODARZI, M., VERDI, J. & MIRZAEI, H. 2016. Glioblastoma: exosome and microRNA as novel diagnosis biomarkers. *Cancer Gene Ther*, 23, 415-418.
- SASI, N. K., TIWARI, K., SOON, F. F., BONTE, D., WANG, T., MELCHER, K., XU, H. E. & WEINREICH, M. 2014. The potent Cdc7-Dbf4 (DDK) kinase inhibitor XL413 has limited activity in many cancer cell lines and discovery of potential new DDK inhibitor scaffolds. *PLoS One*, 9, e113300.
- SAUNDERS, N. A., SIMPSON, F., THOMPSON, E. W., HILL, M. M., ENDO-MUNOZ, L., LEGGATT, G., MINCHIN, R. F. & GUMINSKI, A. 2012. Role of intratumoural heterogeneity in cancer drug resistance: molecular and clinical perspectives. *EMBO Mol Med*, 4, 675-84.

- SCHRODER, L. B. & MCDONALD, K. L. 2015. CDK4/6 Inhibitor PD0332991 in Glioblastoma Treatment: Does It Have a Future? *Front Oncol*, 5, 259.
- SERRES, S., SOTO, M. S., HAMILTON, A., MCATEER, M. A., CARBONELL, W. S., ROBSON, M. D., ANSORGE, O., KHRAPITCHEV, A., BRISTOW, C., BALATHASAN, L., WEISSENSTEINER, T., ANTHONY, D. C., CHOUDHURY, R. P., MUSCHEL, R. J. & SIBSON, N. R. 2012. Molecular MRI enables early and sensitive detection of brain metastases. *Proc Natl Acad Sci U S A*, 109, 6674-9.
- SHUKLA, G., ALEXANDER, G. S., BAKAS, S., NIKAM, R., TALEKAR, K., PALMER, J. D. & SHI, W. 2017. Advanced magnetic resonance imaging in glioblastoma: a review. *Chin Clin Oncol*, 6, 40.
- STRUVE, N., BINDER, Z. A., STEAD, L. F., BREND, T., BAGLEY, S. J., FAULKNER, C., OTT, L., MULLER-GOEBEL, J., WEIK, A. S., HOFFER, K., KRUG, L., RIECKMANN, T., BUSSMANN, L., HENZE, M., MORRISSETTE, J. J. D., KURIAN, K. M., SCHULLER, U., PETERSEN, C., ROTHKAMM, K., DM, O. R., SHORT, S. C. & KRIEGS, M. 2020. EGFRvIII upregulates DNA mismatch repair resulting in increased temozolomide sensitivity of MGMT promoter methylated glioblastoma. *Oncogene*.
- STUPP, R., MASON, W. P., VAN DEN BENT, M. J., WELLER, M., FISHER, B., TAPHOORN, M. J., BELANGER, K., BRANDES, A. A., MAROSI, C., BOGDHANN, U., CURSCHMANN, J., JANZER, R. C., LUDWIN, S. K., GORLIA, T., ALLGEIER, A., LACOMBE, D., CAIRNCROSS, J. G., EISENHAUER, E., MIRIMANOFF, R. O., EUROPEAN ORGANISATION FOR, R., TREATMENT OF CANCER BRAIN, T., RADIO THERAPY, G. & NATIONAL CANCER INSTITUTE OF CANADA CLINICAL TRIALS, G. 2005. Radiotherapy plus concomitant and adjuvant temozolomide for glioblastoma. *N Engl J Med*, 352, 987-96.
- STUPP, R., TAILLIBERT, S., KANNER, A., READ, W., STEINBERG, D., LHERMITTE, B., TOMS, S., IDBAIH, A., AHLUWALIA, M. S., FINK, K., DI MECO, F., LIEBERMAN, F., ZHU, J. J., STRAGLIOTTO, G., TRAN, D., BREM, S., HOTTINGER, A., KIRSON, E. D., LAVY-SHAHAF, G., WEINBERG, U., KIM, C. Y., PAEK, S. H., NICHOLAS, G., BRUNA, J., HIRTE, H., WELLER, M., PALT, Y., HEGI, M. E. & RAM, Z. 2017. Effect of Tumor-Treating Fields Plus Maintenance Temozolomide vs Maintenance Temozolomide Alone on Survival in Patients With Glioblastoma: A Randomized Clinical Trial. *JAMA*, 318, 2306-2316.
- STUPP, R., TAILLIBERT, S., KANNER, A. A., KESARI, S., STEINBERG, D. M., TOMS, S. A., TAYLOR, L. P., LIEBERMAN, F., SILVANI, A., FINK, K. L., BARNETT, G. H., ZHU, J. J., HENSON, J. W., ENGELHARD, H. H., CHEN, T. C., TRAN, D. D., SROUBEK, J., TRAN, N. D., HOTTINGER, A. F., LANDOLFI, J., DESAI, R., CAROLI, M., KEW, Y., HONNORAT, J., IDBAIH, A., KIRSON, E. D., WEINBERG, U., PALT, Y., HEGI, M. E. & RAM, Z. 2015. Maintenance Therapy With Tumor-Treating Fields Plus Temozolomide vs Temozolomide Alone for Glioblastoma: A Randomized Clinical Trial. *JAMA*, 314, 2535-43.
- SUNWOO, H., COLOGNORI, D., FROBERG, J. E., JEON, Y. & LEE, J. T. 2017. Repeat E anchors Xist RNA to the inactive X chromosomal compartment through CDKN1A-interacting protein (CIZ1). *Proc Natl Acad Sci U S A*, 114, 10654-10659.
- SUZUKI, K., YAMAMOTO, M., HASEGAWA, Y., ANDO, M., SHIMA, K., SAKO, C., ITO, G. & SHIMOKATA, K. 2004. Magnetic resonance imaging and computed tomography in the diagnoses of brain metastases of lung cancer. *Lung Cancer*, 46, 357-60.
- SWARTS, D. R. A., STEWART, E. R., HIGGINS, G. S. & COVERLEY, D. 2018. CIZ1-F, an alternatively spliced variant of the DNA replication protein CIZ1 with distinct expression and localisation, is overrepresented in early stage common solid tumours. *Cell Cycle*, 17, 2268-2283.
- SZOPA, W., BURLEY, T. A., KRAMER-MAREK, G. & KASPERA, W. 2017. Diagnostic and Therapeutic Biomarkers in Glioblastoma: Current Status and Future Perspectives. *Biomed Res Int*, 2017, 8013575.

- TAKEDA, M. & NAKAGAWA, K. 2019. First- and Second-Generation EGFR-TKIs Are All Replaced to Osimertinib in Chemo-Naive EGFR Mutation-Positive Non-Small Cell Lung Cancer? *Int J Mol Sci*, 20.
- TAYLOR, J. W., PARIKH, M., PHILLIPS, J. J., JAMES, C. D., MOLINARO, A. M., BUTOWSKI, N. A., CLARKE, J. L., OBERHEIM-BUSH, N. A., CHANG, S. M., BERGER, M. S. & PRADOS, M. 2018. Phase-2 trial of palbociclib in adult patients with recurrent RB1-positive glioblastoma. *J Neurooncol*, 140, 477-483.
- THAKKAR, J. P., DOLECEK, T. A., HORBINSKI, C., OSTROM, Q. T., LIGHTNER, D. D., BARNHOLTZ-SLOAN, J. S. & VILLANO, J. L. 2014. Epidemiologic and molecular prognostic review of glioblastoma. *Cancer Epidemiol Biomarkers Prev*, 23, 1985-96.
- TUMILSON, C. A., LEA, R. W., ALDER, J. E. & SHAW, L. 2014. Circulating microRNA biomarkers for glioma and predicting response to therapy. *Mol Neurobiol*, 50, 545-58.
- URBANSKA, K., SOKOLOWSKA, J., SZMIDT, M. & SYSA, P. 2014. Glioblastoma multiforme - an overview. *Contemp Oncol (Pozn)*, 18, 307-12.
- VERHAAK, R. G., HOADLEY, K. A., PURDOM, E., WANG, V., QI, Y., WILKERSON, M. D., MILLER, C. R., DING, L., GOLUB, T., MESIROV, J. P., ALEXE, G., LAWRENCE, M., O'KELLY, M., TAMAYO, P., WEIR, B. A., GABRIEL, S., WINCKLER, W., GUPTA, S., JAKKULA, L., FEILER, H. S., HODGSON, J. G., JAMES, C. D., SARKARIA, J. N., BRENNAN, C., KAHN, A., SPELLMAN, P. T., WILSON, R. K., SPEED, T. P., GRAY, J. W., MEYERSON, M., GETZ, G., PEROU, C. M., HAYES, D. N. & CANCER GENOME ATLAS RESEARCH, N. 2010. Integrated genomic analysis identifies clinically relevant subtypes of glioblastoma characterized by abnormalities in PDGFRA, IDH1, EGFR, and NF1. *Cancer Cell*, 17, 98-110.
- VOITENLEITNER, C., FANNING, E. & NASHEUER, H. P. 1997. Phosphorylation of DNA polymerase alpha-primase by cyclin A-dependent kinases regulates initiation of DNA replication in vitro. *Oncogene*, 14, 1611-5.
- VOITENLEITNER, C., REHFUESS, C., HILMES, M., O'REAR, L., LIAO, P. C., GAGE, D. A., OTT, R., NASHEUER, H. P. & FANNING, E. 1999. Cell cycle-dependent regulation of human DNA polymerase alpha-primase activity by phosphorylation. *Mol Cell Biol*, 19, 646-56.
- WALTER, D., HOFFMANN, S., KOMSELI, E. S., RAPPSILBER, J., GORGOULIS, V. & SORENSEN, C. S. 2016. SCF(Cyclin F)-dependent degradation of CDC6 suppresses DNA re-replication. *Nat Commun*, 7, 10530.
- WANG, D. Q., WANG, K., YAN, D. W., LIU, J., WANG, B., LI, M. X., WANG, X. W., LIU, J., PENG, Z. H., LI, G. X. & YU, Z. H. 2014. Ciz1 is a novel predictor of survival in human colon cancer. *Exp Biol Med (Maywood)*, 239, 862-870.
- WEN, P. Y. & KESARI, S. 2008. Malignant gliomas in adults. *N Engl J Med*, 359, 492-507.
- WU, C. X., LIN, G. S., LIN, Z. X., ZHANG, J. D., LIU, S. Y. & ZHOU, C. F. 2015. Peritumoral edema shown by MRI predicts poor clinical outcome in glioblastoma. *World J Surg Oncol*, 13, 97.
- WU, J., LEI, L., GU, D., LIU, H. & WANG, S. 2016. CIZ1 is upregulated in hepatocellular carcinoma and promotes the growth and migration of the cancer cells. *Tumour Biol*, 37, 4735-42.
- YARDIMCI, H. & WALTER, J. C. 2014. Prereplication-complex formation: a molecular double take? *Nat Struct Mol Biol*, 21, 20-5.
- YIN, J., WANG, C., TANG, X., SUN, H., SHAO, Q., YANG, X. & QU, X. 2013. CIZ1 regulates the proliferation, cycle distribution and colony formation of RKO human colorectal cancer cells. *Mol Med Rep*, 8, 1630-4.
- ZHANG, D., WANG, Y., DAI, Y., WANG, J., SUO, T., PAN, H., LIU, H., SHEN, S. & LIU, H. 2015. CIZ1 promoted the growth and migration of gallbladder cancer cells. *Tumour Biol*, 36, 2583-91.
- ZHANG, S., CHANG, L., ALFIERI, C., ZHANG, Z., YANG, J., MASLEN, S., SKEHEL, M. & BARFORD, D. 2016. Molecular mechanism of APC/C activation by mitotic phosphorylation. *Nature*, 533, 260-264.

- ZHOU, X., LIU, Q., WADA, Y., LIAO, L. & LIU, J. 2018. CDKN1A-interacting zinc finger protein 1 is a novel biomarker for lung squamous cell carcinoma. *Oncol Lett*, 15, 183-188.
- ZHU, P., DU, X. L., LU, G. & ZHU, J. J. 2017. Survival benefit of glioblastoma patients after FDA approval of temozolomide concomitant with radiation and bevacizumab: A population-based study. *Oncotarget*, 8, 44015-44031.
- ZITRON, I. M., THAKUR, A., NORKINA, O., BARGER, G. R., LUM, L. G. & MITTAL, S. 2013. Targeting and killing of glioblastoma with activated T cells armed with bispecific antibodies. *BMC Cancer*, 13, 83.